CERN – EUROPEAN ORGANIZATION FOR NUCLEAR RESEARCH

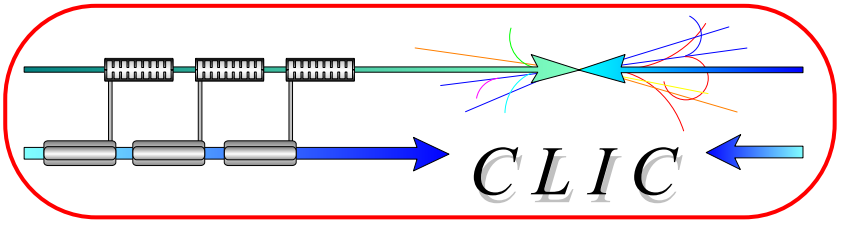

CLIC-Note-333
CERN/PS/97-051

SCALING LAWS FOR e+/e- LINEAR COLLIDERS

J-P. Delahaye, G. Guignard, T. Raubenheimer, I. Wilson
CERN, Geneva, Switzerland

Abstract

Design studies of a future TeV e+e- Linear Collider (TLC) are presently being made by five major laboratories within the framework of a world-wide collaboration. A figure of merit is defined which enables an objective comparison of these different designs. This figure of merit is shown to depend only on a small number of parameters. General scaling laws for the main beam parameters and linac parameters are derived and prove to be very effective when used as guidelines to optimize the linear collider design. By adopting appropriate parameters for beam stability, the figure of merit becomes nearly independent of accelerating gradient and RF frequency of the accelerating structures. In spite of the strong dependence of the wake-fields with frequency, the single bunch emittance preservation during acceleration along the linac is also shown to be independent of the RF frequency when using equivalent trajectory correction schemes. In this situation, beam acceleration using high frequency structures becomes very advantageous because it enables high accelerating fields to be obtained, which reduces the overall length and consequently the total cost of the linac.

Geneva, Switzerland
(1997)

SCALING LAWS for e^+/e^- LINEAR COLLIDERS

J.P. Delahaye, G. Guignard, T. Raubenheimer and I. Wilson

Abstract

Design studies of a future TeV e^+e^- Linear Collider (TLC) are presently being made by five major laboratories within the framework of a world-wide collaboration. A figure of merit is defined which enables an objective comparison of these different designs. This figure of merit is shown to depend only on a small number of parameters. General scaling laws for the main beam parameters and linac parameters are derived and prove to be very effective when used as guidelines to optimize the linear collider design. By adopting appropriate parameters for beam stability, the figure of merit becomes nearly independent of accelerating gradient and RF frequency of the accelerating structures. In spite of the strong dependence of the wake-fields with frequency, the single bunch emittance preservation during acceleration along the linac is also shown to be independent of the RF frequency when using equivalent trajectory correction schemes. In this situation, beam acceleration using high frequency structures becomes very advantageous because it enables high accelerating fields to be obtained, which reduces the overall length and consequently the total cost of the linac.

1. Introduction

A 1 TeV, high luminosity (10^{34} $cm^{-2}sec^{-1}$) e^+/e^- Linear Collider (TLC) is strongly supported by the physics community as a possible future complementary facility to the recently approved 14 TeV Large Hadron Collider (LHC). These TLC parameters are very challenging since the luminosity is three orders of magnitude larger than that of the only linear collider presently in operation (the SLC at SLAC) and the colliding beam energy is ten times higher. Five different laboratories are studying the TLC option as part of a world wide collaboration [1]. The various possible approaches and technologies that are being explored, are discussed and compared periodically in international workshops. This report derives general scaling laws for multi-bunch operation of normal conducting travelling-wave accelerating structures; for this reason, both the TESLA super-conducting design and the VLEPP single bunch design are excluded from the comparisons although they are often included in the graphs for completeness.

The luminosity of an e^+/e^- linear collider is given as follows (all parameters used in this report are defined in Appendix 1):

$$L = \frac{k_b N_b^2 f_{rep}}{4\pi \bar{\sigma}_x^* \bar{\sigma}_y^*} = \frac{N_b P_b}{4\pi e U_f \bar{\sigma}_x^* \bar{\sigma}_y^*} = \frac{H_D}{4\pi e} \frac{N_b}{U_f} \frac{P_b}{\sigma_x^* \sigma_y^*} \qquad (1)$$

In order to reach the specified luminosity of $10^{34}\,cm^{-2}sec^{-1}$ at an energy, $2U_f$, of 1 TeV c.m., a future TLC will have to collide very low emittance beams with several MW of power, P_b, focused down to transverse sizes, $\sigma^*_{x,y}$, of a few nm at the interaction point (I.P.). The enhancement factor, H_D, takes into account the reduction of the nominal beam size by the strong electromagnetic disruptive field of the dense opposing bunch at the I.P. When colliding electrons and positrons, the so-called "pinch effect" helps to increase the integrated luminosity by a mutual focusing of the bunches. This effect has however to be limited as it generates synchrotron radiation by beamstrahlung which has two detrimental effects on the experimental physics conditions: first it induces a momentum spread within the bunch which broadens the luminosity/energy spectrum and secondly it leads to the creation of e^+/e^- pairs, a potential source of background in the detector. The broadening of the luminosity/energy spectrum is characterized by the average beam energy loss parameter, δ_B, and the background level in the detector by the average number of photons radiated per electron, n_γ. Both are related to the beamstrahlung parameter, Y, a measure of the electromagnetic field strength of the bunches [2,3]. As pointed out in Appendix 2 (equations A2-12 and A2-13), in the low beamstrahlung regime, the momentum spread induced by beamstrahlung and the number of radiated photons can be approximated by:

$$\delta_B \propto \frac{U_f}{\sigma_z}\frac{N_b^2}{\left(\bar{\sigma}_x^* + \bar{\sigma}_y^*\right)^2} \propto \frac{U_f}{\sigma_z}\frac{N_b^2}{\bar{\sigma}_x^{*2}} \qquad \text{and} \qquad n_\gamma \propto \frac{N_b}{\bar{\sigma}_x^* + \bar{\sigma}_y^*} \propto \frac{N_b}{\bar{\sigma}_x^*} \propto \left(\frac{\sigma_z \delta_B}{U_f}\right)^{1/2} \qquad (2)$$

It is therefore possible using a flat beam at the I.P. ($\sigma_y << \sigma_x$) to both maximize the luminosity and to limit δ_B and n_γ. If, in addition, the effective beam sizes obtained by the "hour-glass" effect are optimized by adjusting the vertical focusing function, β_y^*, at the I.P. to be equal to the bunch length, σ_z, then ***the luminosity only depends on a surprisingly small number of beam parameters as shown in Appendix 2 (equation A2-19):***

$$\boxed{L \propto \left(H_{Dy}\right)^{f\left(\frac{\sigma_x^*}{\sigma_y^*}\right)} \frac{\delta_B^{1/2} P_b}{U_f \varepsilon_{ny}^{*1/2}}} \qquad (3)$$

namely the final beam energy, U_f, the average energy loss by beamstrahlung, δ_B, the beam power per linac, P_b, and the normalized vertical emittance ε_{ny}^* at the I.P. For small values of δ_B (typically a few percent), the enhancement factor, H_{Dy}, is limited to values between 1 and 2 in all TLC designs (see Tables 1 and 2).

2. Figure of merit in the low beamstrahlung regime

A figure of merit is defined which enables an objective comparison of the different designs. The figure of merit, M, is defined as the luminosity at a given beam energy normalized to the AC power consumption and the momentum spread δ_B. The colliding beam energy and the acceptable momentum spread are imposed by experimental physics considerations, and the AC power consumption is limited by the TLC exploitation cost. In principle, the figure of merit should also be normalised to the TLC capital cost but this information for the moment is not available. Introducing the AC power to beam conversion efficiency in equation (3),

$$P_b = \eta_b^{AC} P_{AC} \tag{4}$$

and neglecting the enhancement factor, the figure of merit in the low beamstrahlung regime (where all present studies are made [1]), only depends on two parameters η_b^{AC} and ε_{ny}^{*} :

$$\boxed{M = L\frac{U_f}{\delta_B^{1/2} P_{AC}} \propto \frac{\eta_b^{AC}}{\varepsilon_{ny}^{*1/2}}} \tag{5}$$

The figures of merit, and the corresponding beam parameters (taken from Table1), for the different schemes being studied are compared in Figs.1 and 2 respectively.

The AC power to beam power conversion efficiency is the product of the AC to RF power efficiency and the RF to beam power efficiency:

$$\eta_b^{AC} = \eta_{RF}^{AC} \times \eta_b^{RF} \tag{6}$$

An impressive world-wide technological R&D program is presently being pursued to develop advanced and efficient high peak power RF sources. In spite of the large range of frequencies and technologies being explored, the AC to RF power conversion efficiency is fairly constant around 35% for all the different TLC designs (see Tables 1 and 2). Assuming the AC to RF power conversion efficiency is the same for all the designs, the figure of merit becomes:

$$M \propto \frac{\eta_{RF}^{AC} \times \eta_b^{RF}}{\varepsilon_{ny}^{*1/2}} \propto \frac{\eta_b^{RF}}{\varepsilon_{ny}^{*1/2}} \tag{7}$$

The optimisation of the design of a TLC consists of selecting the beam parameters, and choosing a technology that is able to accelerate, at a reasonable cost, a high power beam with an optimum AC power to beam power conversion efficiency *(see chapters 3 and 4)* ***while maintaining the vertical normalised beam emittance as small as possible*** *(see chapters 5 to 7).*

Fig. 1: Luminosity and figure of merit in the TLC designs at 500 (●) and 1000 (▲) GeV c.m.

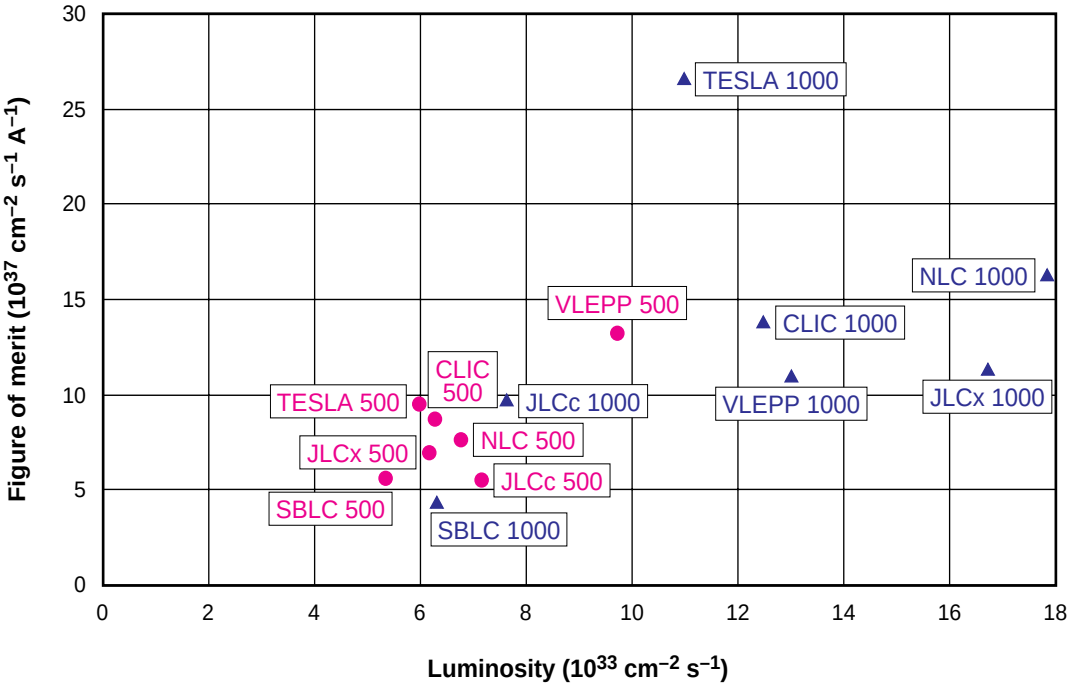

Fig. 2: Power efficiency and vertical beam emittance in the TLC designs at 500 (●) and 1000 (▲) GeV c.m.

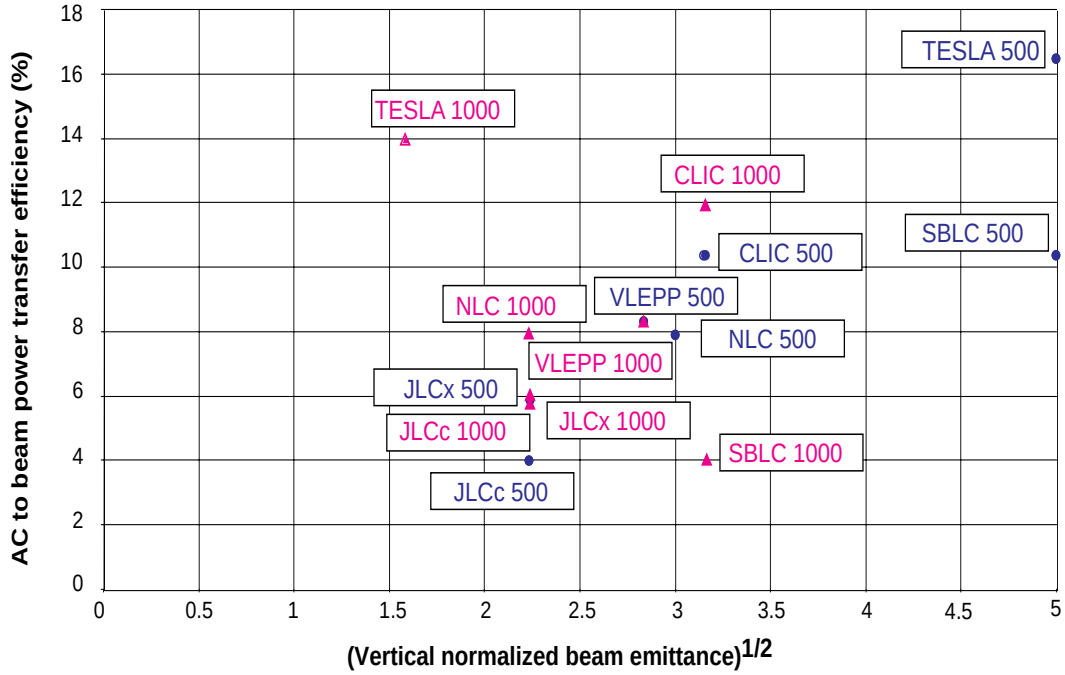

3. The RF Power to Beam Conversion efficiency

The RF to beam conversion efficiency is directly related to the choice of the RF frequency and the beam parameters. As shown in Appendix 3 (equation A3-16) for normal conducting, constant gradient, travelling wave accelerating structures, it is given by:

$$\eta_b^{RF} = \frac{2g(\tau)}{\left[1-\frac{e^{-2\tau}}{g(\tau)}\right]} \times \frac{k_b \Delta_b \omega}{Q\left[1+\frac{(k_b-1)\Delta_b \omega}{2Q\tau(1-\delta)^2}\right]} \times \frac{\delta}{(1-\delta)} \tag{8}$$

where δ is the beam loading parameter (equation A3-13):

$$\delta = \frac{G_u - G_a}{G_u} = \frac{\frac{J}{2}\left[1-\frac{e^{-2\tau}}{g(\tau)}\right]}{1+\frac{J}{2}\left[1-\frac{e^{-2\tau}}{g(\tau)}\right]} \tag{9}$$

g(τ) is a function of the field attenuation constant per accelerating structure, τ, for an assumed "constant gradient" geometry:

$$g(\tau) = \frac{1-e^{-2\tau}}{2\tau} \tag{10}$$

and J is the so-called dimensionless normalised beam current (equation A3-14):

$$J = \frac{R' q_b}{G_a \Delta_b} = \frac{R' I_b}{G_a} \tag{11}$$

where R', G_a and I_b are respectively the shunt impedance per meter, the loaded accelerating gradient and the beam current.

In order to obtain a high RF to beam transfer efficiency, all TLC designs (except VLEPP) have chosen to operate with a large number of bunches to be close to the field equilibrium regime in the accelerating structures. In the extreme case of an infinite number of bunches, the formulation (see Appendix 3) becomes extremely simple with the RF to beam efficiency depending only on the field attenuation constant and the normalised beam current (equation A3-21):

$$\eta_b^{RF} = \frac{2\tau g(\tau) J}{\left[1+\frac{J}{2}\left(1-\frac{e^{-2\tau}}{g(\tau)}\right)\right]^2} \tag{12}$$

For a given value of J, there is a value τ_{opt} which maximises the RF to beam efficiency (Equation A3-22):

$$\tau_{opt} = \frac{G_u \Delta_b}{R' q_b} = \frac{1}{J(1-\delta)} \qquad (13)$$

The variations of these parameters together with the corresponding beam loading parameters are shown in Figs. A2 to A5.

Using accelerating structures with an optimum field attenuation, τ_{opt}, following equation (13), and for the more usual range of beam parameters where the beam loading parameter δ is limited to 50% (Fig. 3), the scaling of η_b^{RF} and τ_{opt} is approximated by:

$$0.5 \le J \le 2 \Rightarrow \qquad \eta_b^{RF} \propto (J)^{1/2} = \left(\frac{R' q_b}{G_a \Delta_b} \right)^{1/2} \text{ and } \quad \tau_{opt} \propto J^{-9/10} \qquad (14)$$

Here, $\propto$ is the approximate proportionality implied by the straight line fit in Fig. 3 over the range of parameters considered.

Fig. 3: Optimum RF to beam efficiency and beam loading parameters as a function of the normalized beam current

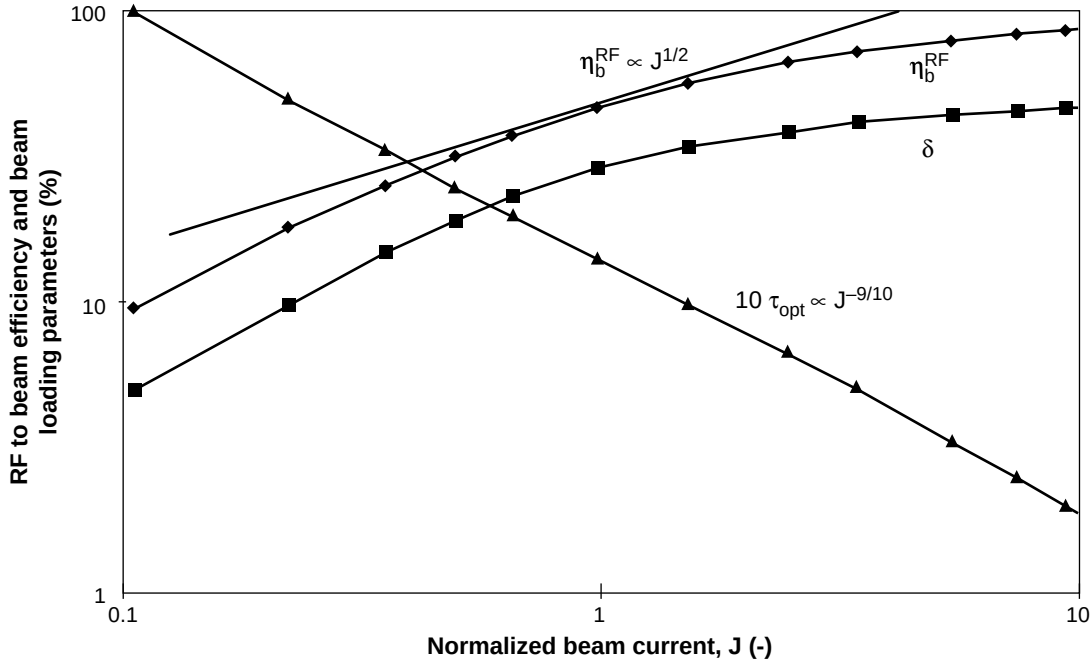

The figure of merit then becomes:

$$M \propto \frac{\eta_b^{RF}}{\varepsilon_{ny}^{*1/2}} \propto \left(\frac{J}{\varepsilon_{ny}^{*}} \right)^{1/2} = \left(\frac{R' q_b}{\varepsilon_{ny}^{*} G_a \Delta_b} \right)^{1/2} \qquad (15)$$

To optimise the design of a linear collider therefore the beam and linac parameters should be chosen to maximise the J parameter (see chapter 4), while preserving the initial vertical normalised beam emittance (see chapter 5).

4. The normalised beam current, J

All four parameters in the expression for J, (equation 11) are directly related to the RF frequency, ω, of the accelerating structures. This explains why the different TLC designs are mostly frequency driven.

$$J = \frac{R'q_b}{G_a\Delta_b} \propto \frac{R'N_b}{G_a\Delta_b} \qquad (16)$$

• The well known variation with frequency of the normalised shunt impedance per unit length, R',[4] is shown in Fig.4 to hold for the various TLC designs when taking into account the variation of R' with the iris to wavelength ratio a/λ :

$$r' = \frac{r}{L_s} \propto \omega(a/\lambda)^{-1} \text{ and } Q \propto \omega^{-1/2} \Rightarrow R' = r'Q \propto \omega^{1/2}(a/\lambda)^{-1} \qquad (17)$$

Fig. 4: Variation of the shunt impedances and quality factors of the accelerating structures in the TLC designs

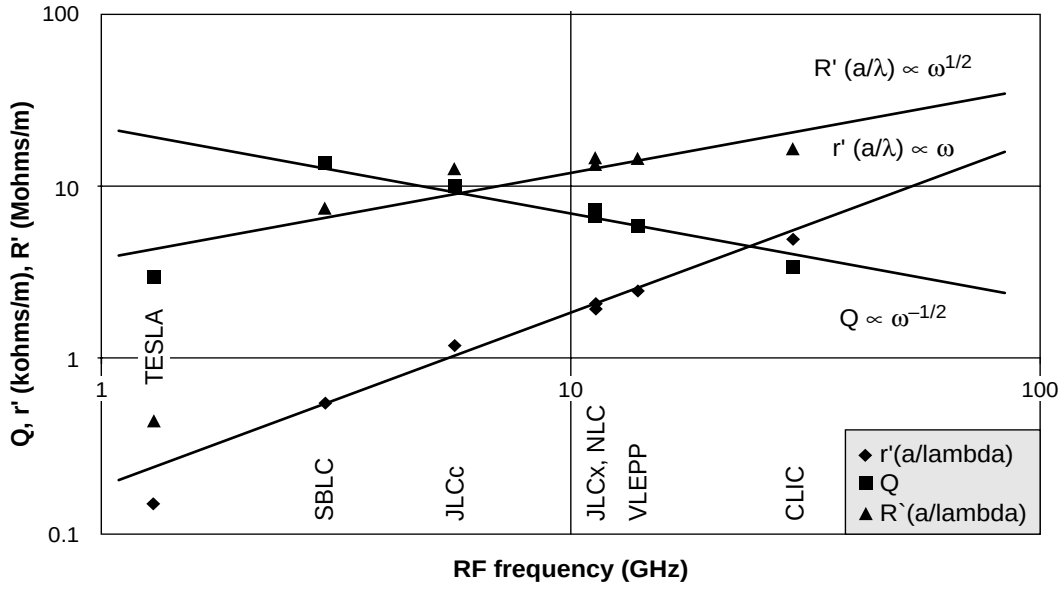

•The minimum distance between bunches is limited by the transverse wake-field level that can be obtained at the second and subsequent bunches by damping and/or detuning. The number of RF periods to obtain the same relative wake-field reduction for a given type of structure when scaled to other frequencies is the same. This is why, as shown in Fig. 5 and in spite of the different structure designs, the distance between bunches adopted in the various TLC designs scales with the RF wavelength:

$$\Delta_b \propto \omega^{-1} \qquad (18)$$

Here again, $\propto$ is the approximate proportionality implied by the straight line fit in Fig. 5.

Fig. 5: Time interval between bunches in the TLC designs

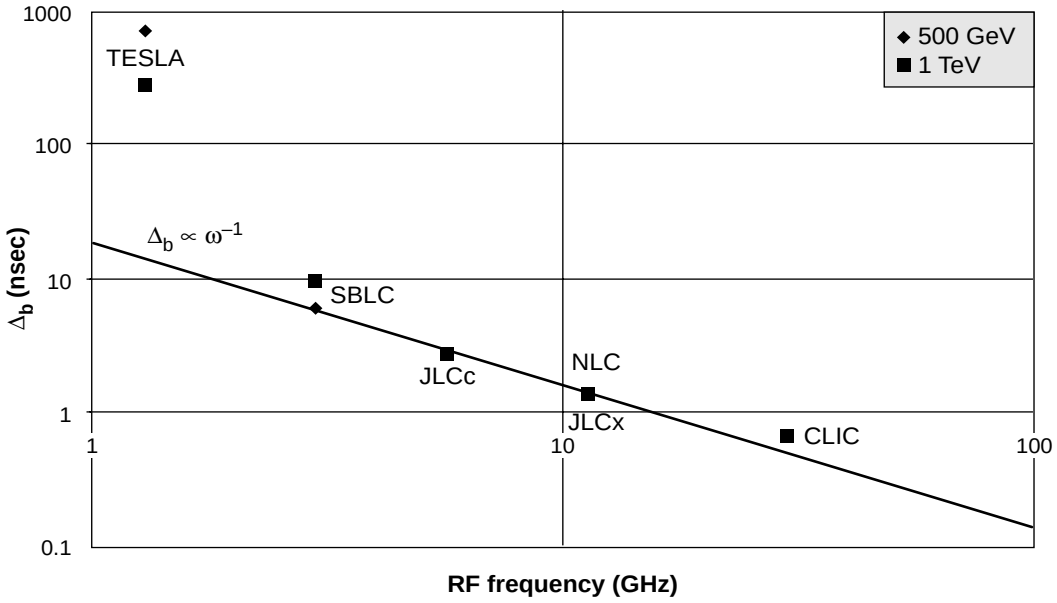

Introducing equations (17) and (18) into equation (16), the J parameter becomes:

$$J = \frac{R' q_b}{G_a \Delta_b} \propto \omega^{3/2} (a/\lambda)^{-1} G_a^{-1} N_b \qquad (19)$$

The charge per bunch should be as high as possible to maximise J. Its maximum value is limited by beam stability and vertical beam emittance considerations as developed in chapter 5.

5. Beam stability and the vertical beam emittance, ε_{ny}^*

Vertical normalised beam emittances of a few 10^{-8} rad-m can be produced by state-of-the-art damping rings. During injection and acceleration along the several kilometer-long main linacs however, the beams suffer transverse blow-up $\Delta\varepsilon_n$, which is especially important in the vertical plane because of the particularly small initial emittance. After filamentation in the linac and emittance dilution in the beam delivery, the vertical normalised emittance at the end of the linac, ε_{ny}, and at the final focus, ε_{ny}^*, are deduced from the normalised emittance, ε_{nyo}, at injection into the linac:

$$\varepsilon_{ny}^* \propto \varepsilon_{ny} = \varepsilon_{nyo} + \Delta\varepsilon_{ny} \qquad (20)$$

One of the primary causes of emittance blow-up comes from the transverse wake-fields induced by the misalignment of the accelerating structures and of the beam trajectory. The overall emittance blow-up is taken as the sum of both contributions:

$$\left(\Delta\varepsilon_{ny}\right)^2 \cong \left(\Delta\varepsilon_{ny}\right)_{RF}^2 + \left(\Delta\varepsilon_{ny}\right)_{BPM}^2 \qquad (21)$$

where:

- $\left(\Delta\varepsilon_{ny}\right)_{RF}$ is the beam dilution due to the r.m.s. misalignment of the accelerating structures, $\left\langle \Delta y_{RF} \right\rangle$, assuming perfect beam trajectory alignment,
- $\left(\Delta\varepsilon_{ny}\right)_{BPM}$ is the beam dilution induced by the residual beam trajectory oscillations after correction when limited by the Beam Position Monitor (BPM) misalignment, $\left\langle \Delta y_{BPM} \right\rangle$.

Wake-fields deteriorate the beam quality during acceleration:

- in the longitudinal plane by introducing momentum spread along each bunch, and from bunch to bunch;
- in the transverse planes by single-bunch and multi-bunch Beam Break-Up (BBU) producing emittance blow-up.

These effects are especially strong in high frequency structures because longitudinal and transverse wake-fields scale with the second and third power of the frequency respectively.

5.1 BNS damping:

The single-bunch beam stability is greatly improved by the so-called Balakin, Novokhatsky and Smirnov (BNS) damping [5]: A correlated energy spread is created along the bunch from head to tail by off-crest acceleration on the RF wave. This results in an increased focusing of the tail of the bunch with respect to the head and compensates the opposing defocusing effects due to transverse wake-fields and breaks the resonant condition between the head and the tail of the bunch such that:

$$\Delta p / p = \delta_{BNS} \tag{22}$$

The necessary momentum spread for BNS damping is given by [5,6]:

$$\delta_{BNS} \propto N_b \left\langle W_T \right\rangle \frac{\langle\beta\rangle\left\langle L_{CELL}\right\rangle}{U} \tag{23}$$

where $\left\langle \beta \right\rangle$ is the mean betatron amplitude of the focusing optics along the linac, which is usually based on a FODO lattice with a cell length, L_{CELL}, and which scales with the beam energy, U, (when the phase advance is constant) following:

$$\frac{\left\langle \beta \right\rangle}{\left\langle \beta_0 \right\rangle} = \frac{\left\langle L_{CELL} \right\rangle}{\left\langle L_{0CELL} \right\rangle} = \left(\frac{U}{U_0} \right)^{\alpha} \quad \text{with} \quad \alpha \cong 1/2 \Rightarrow \frac{\langle\beta\rangle\left\langle L_{CELL}\right\rangle}{U} \propto \frac{\langle\beta_o\rangle^2}{U_o} \tag{24}$$

$\left\langle W_T \right\rangle$ is the short range transverse wake-field averaged over the bunch which, following [7], scales as:

$$\left\langle W_T \right\rangle \propto W_T' \sigma_z \propto \omega^4 \left(a/\lambda\right)^{-7/2} \sigma_z \tag{25}$$

Different authors give different descriptions where $\langle W_T \rangle$ scales as $\sigma_z^{1/2}$ or $(a/\lambda)^{-4}$. For a short bunch in an infinitely long periodic structure the deflection should be proportional to σ_z and this is the description retained in equation (25). However, a bunch with a finite length sees some of the curvature of the wake-field. As a consequence, the averaged transverse wake-field scales less rapidly than σ_z and in practice lays somewhere between σ_z and $\sigma_z^{1/2}$.

The BNS energy spread, δ_{BNS}, provides a convenient measure of the effect of the wake-fields on the transverse beam dynamics. Introducing equations (24) and (25) into (23), it becomes:

$$\delta_{BNS} \propto N_b \sigma_z \beta_o^2 (a/\lambda)^{-7/2} \omega^4 \tag{26}$$

Under BNS damping conditions, the corresponding vertical blow-ups are given by [6,8]:

$$(\Delta\varepsilon_{ny})_{RF} \propto (N_b \langle W_T \rangle)^2 \frac{\langle \Delta y_{RF}^2 \rangle}{G_a} \frac{\langle \beta_o \rangle L_s}{\alpha} \left[\left(\frac{U_f}{U_o} \right)^{\alpha} - 1 \right] \tag{27}$$

$$(\Delta\varepsilon_{ny})_{BPM} \propto (N_b \langle W_T \rangle)^2 \frac{\langle \Delta y_{BPM}^2 \rangle}{G_a} \frac{L_{oCELL}^2}{\alpha} \left[\left(\frac{U_f}{U_o} \right)^{2\alpha} - 1 \right] \tag{28}$$

Substituting equations (24), (25) and (26) in equations (27) and (28) gives the following beam dilutions along the linac for the same final beam energy, U_f, and the same focusing optics scaling, α:

$$(\Delta\varepsilon_{ny})_{RF} \propto N_b^2 \sigma_z^2 (a/\lambda)^{-7} \omega^8 G_a^{-1} \langle \beta_0 \rangle L_s \langle \Delta y_{RF}^2 \rangle \propto \delta_{BNS}^2 G_a^{-1} \langle \beta_o \rangle^{-3} L_s \langle \Delta y_{RF}^2 \rangle \tag{29}$$

$$(\Delta\varepsilon_{ny})_{BPM} \propto N_b^2 \sigma_z^2 (a/\lambda)^{-7} \omega^8 G_a^{-1} \langle \beta_0 \rangle^2 \langle \Delta y_{BPM}^2 \rangle \propto \delta_{BNS}^2 G_a^{-1} \langle \beta_o \rangle^{-2} \langle \Delta y_{BPM}^2 \rangle \tag{30}$$

The above equations point out the strong dependence of the blow-up induced by the transverse wake-fields with the power eight of the frequency. But the other parameters in equations (29) and (30) also scale strongly with the frequency.

The dependence with the frequency and the accelerating gradient of the other parameters, N_b, σ_z, a/λ, $\langle \beta_o \rangle$ L_s, $\langle \Delta y_{RF} \rangle$, and $\langle \Delta y_{BPM} \rangle$ have now to be determined. The beam blow-ups in the various TLC designs [1] are all reasonably small at the level of a few tens of percent. Equation (29) has been used to calculate the blow up induced by transverse wake-fields for the different TLC designs using the most up-to-date parameters and assuming equivalent beam based correction schemes

(Tables 1 and 2). As shown in Fig. 6, and in spite of the broad RF frequency range, the absolute values of the transverse blow-up are all very comparable (except for TESLA and VLEPP because their charges per bunch are respectively well below, and well above, the BNS damping condition), which justifies the following assumption :

$$\boxed{\Delta\varepsilon_{ny} = Const.} \qquad (31)$$

Fig. 6: Calculated blow-up from transverse wake-fields (arbitrary scale)

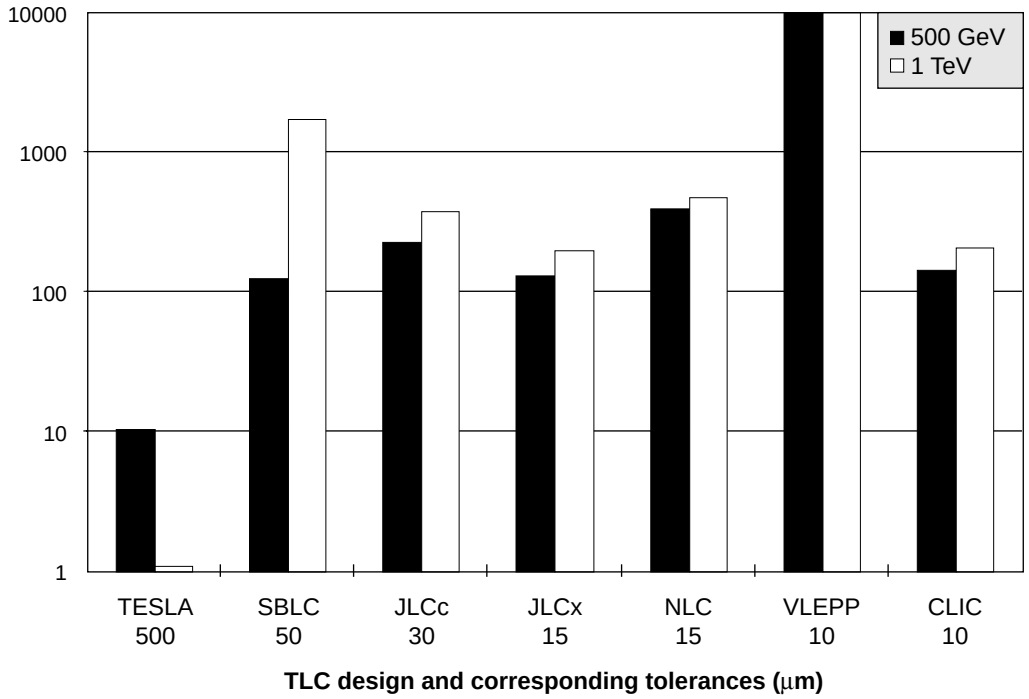

5.2 Bunch length:

The bunch length, σ_z, is made as small as possible in order to minimise the transverse wake-field according to equation (25). It is limited by the necessity to reduce the momentum spread along the bunch as much as possible at the end of the linac in order to match the beam delivery and final focus acceptance which is usually limited to a few per-mil. The momentum spread along the bunch induced by the short range longitudinal wake-field is reduced by running off the crest of the RF wave in the last part of the linac such that [8]:

$$\left(\frac{\Delta p}{p}\right)_f \approx \frac{1.25}{\cos(\Phi_{RF})}\left(\frac{2\pi\varepsilon_o r_e N_b W_L}{G_a} - \frac{3\sigma_z \omega \sin(\Phi_{RF})}{2c}\right) \approx 0 \qquad (32)$$

where Φ_{RF} is the off-crest RF phase and W_L is the short range longitudinal wake-field given by [7]:

$$W_L \propto (a/\lambda)^{-2}\omega^2 \qquad (33)$$

Limiting the off-crest RF phase to small values for efficient beam acceleration and substituting equation (33) in equation (32):

$$\sigma_z \propto N_b G_a^{-1} (a/\lambda)^{-2} \omega \qquad (34)$$

5.3 Ratio of iris radius of accelerating structures to RF wavelength:

As shown in Fig. 7 for the different TLC designs, the ratio of iris radius to RF wavelength, a/λ, increases with increasing frequency in order to minimise the effect of the transverse wake fields (equation 25):

$$a/\lambda \propto \omega^{1/5} \qquad (35)$$

Here, $\propto$ is the approximate proportionality implied by the straight line fit in Fig. 7.

Fig. 7: Iris to wavelength ratio in the TLC designs

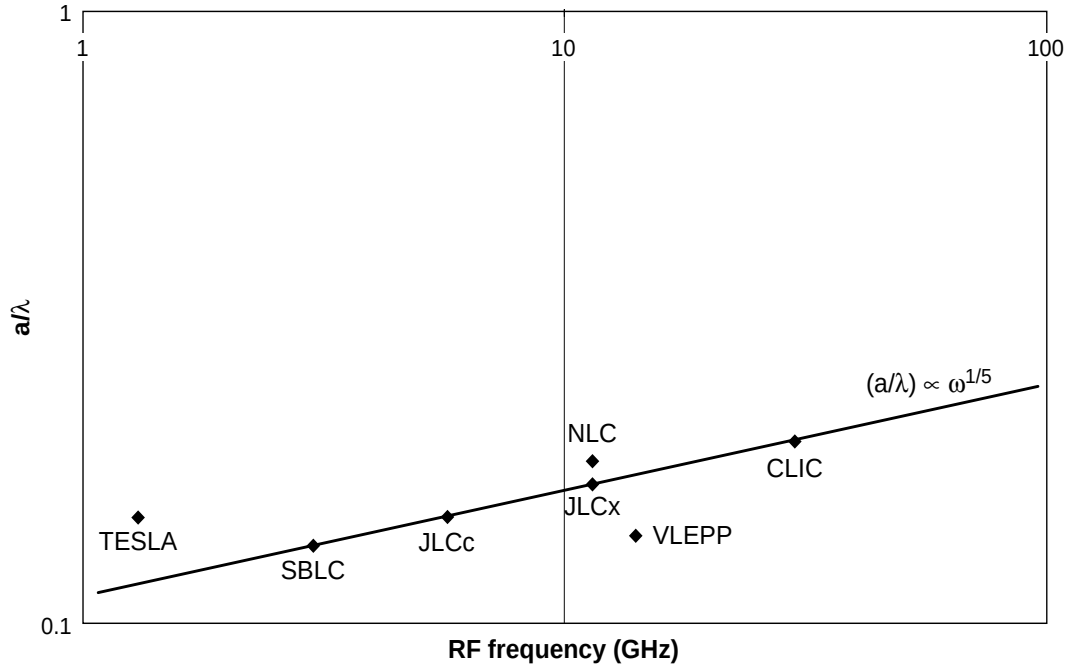

5.4 Focusing optics of the linacs:

In order to limit the BNS momentum spread for beam stability (equation 26), the focusing strength of the FODO cell lattice is usually increased with the operating frequency as shown in Fig. 8. This is possible at higher frequencies because of the reduction in size of the linac components. Assuming the inner diameter, Φ, of the quadrupoles is scaled inversely with frequency in the same way as the inner radius of the iris, a, of the RF structures:

$$\Phi \propto a \propto (a/\lambda)\omega^{-1} \qquad (36)$$

then for the same magnetic field on the poles, B, the same phase advance per cell, and the same quadrupole filling factor, F, the FODO cell length, L_{cell}, scales as follows:

$$L_{cell} \propto \frac{L_{quad}}{F} \propto \frac{\Phi}{FL_{cell}B} \propto \frac{(a/\lambda)}{FL_{cell}B\omega} \quad \Rightarrow \quad L_{cell} \propto \left(\frac{(a/\lambda)}{FB\omega}\right)^{1/2} \qquad (37)$$

and since $\langle\beta\rangle \propto L_{cell} \quad \Rightarrow \quad \langle\beta_o\rangle \propto (a/\lambda)^{1/2}\omega^{-1/2} \propto \omega^{-2/5}$ (38)

Fig. 8: Optics focusing at injection into the TLC designs

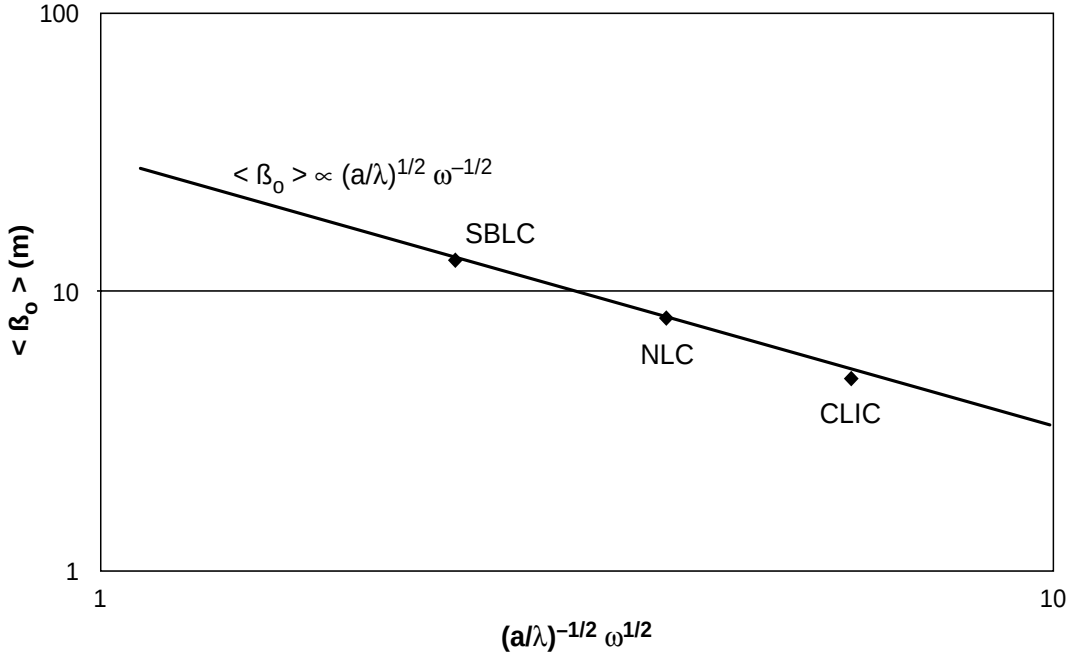

5.5 Pre-Alignment tolerances of the RF structures:

Because the size of accelerating structures becomes smaller with increasing frequency, the accuracy with which they can be made and pre-aligned is expected to scale approximately with the inverse of the frequency. As seen in Fig. 9, the variation of the pre-alignment tolerances of the RF structures for the various TLC designs is well approximated by the following scaling law with frequency:

$$\langle \Delta y_{RF} \rangle \propto \omega^{-3/4} \qquad (39)$$

Fig. 9: Alignment tolerances in the TLC designs

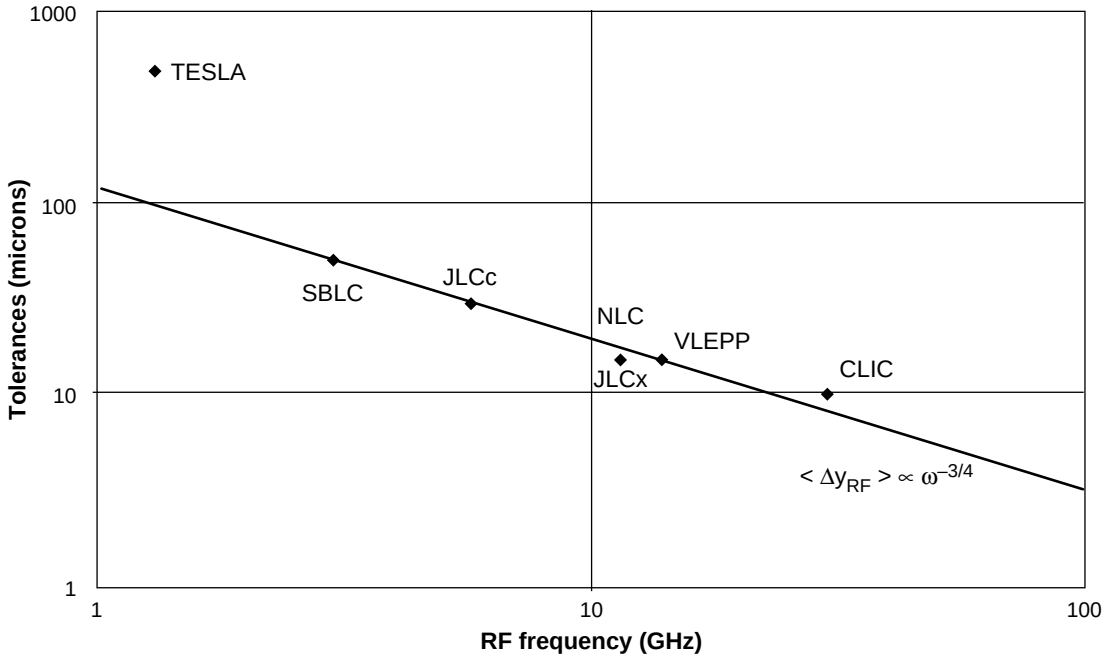

5.6 Accelerating section length:

The length of the accelerating section, L_s, is adjusted to have the optimum field attenuation parameter, τ_{opt}, which maximises the RF to beam efficiency according to equation (A3-22) as developed in Appendix 3, in the extreme case of an infinite number of bunches:

$$L_s = \frac{2Qv_g\tau_{opt}}{\omega} = \frac{2Qv_g}{\omega J(1-\delta)} \qquad (40)$$

Neglecting the variation of the beam loading parameter, δ, for small δ values, which corresponds to a 10% approximation of the exponent of J in the expression for τ_{opt} with $\tau_{opt} \propto J^{-1}$ instead of $\tau_{opt} \propto J^{-0.9}$ as observed in Fig.3 and derived in equation (14), the scaling of the optimum length of the accelerating structure becomes:

$$L_s = \frac{2Qv_g\tau_{opt}}{\omega} \propto \frac{2Qv_g}{\omega J} \qquad (41)$$

The normalised beam current, J, (equation 11), scales according to equation (19) as demonstrated in chapter 4:

$$J = \frac{R'q_b}{G_a\Delta_b} \propto \omega^{3/2}(a/\lambda)^{-1}G_a^{-1}N_b \qquad (42)$$

The group velocity is approximated by:

$$v_g \propto (a/\lambda)^3 \tag{43}$$

which corresponds to the best fit of the expression derived in [9]:

$$v_g / c = \exp\left\{3.1 - 2.4(a/\lambda)^{-1/2} - 0.9(a/\lambda)\right\} \tag{44}$$

The quality factor follows the standard relation [4], $Q \propto \omega^{-1/2}$, from equation (17) (Fig. 4).

Introducing equations (17), (42), and (43) into equation (41), the optimum length of the accelerating sections, in the extreme case of an infinite number of bunches, becomes:

$$L_s \propto \omega^{-3}(a/\lambda)^4 G_a N_b^{-1} \tag{45}$$

5.7 Charge per bunch

It is now finally possible to derive the scaling of the maximum charge per bunch. This is the charge which produces a small and tolerable beam blow-up induced by the misalignment of the RF structures according to condition (31). It is deduced by substituting the relations found above for the scaling of the different parameters (equations 34, 35, 38, 39 and 45) into the equation (29):

$$\left(\Delta\varepsilon_{ny}\right)_{RF} \propto Const. \qquad \Rightarrow \qquad N_b \propto \omega^{-11/6}(a/\lambda)^{7/3} G_a^{2/3} \beta_o^{-1/3} \tag{46}$$

6. Scaling laws of the main beam and linac parameters

Now that the frequency dependence of the maximum charge per bunch has been derived (equation 46), the scaling laws for the main beam and linac parameters can be deduced first for the general case and then with the assumption that the focusing optics along the linac follows equation (38) and that the iris to wavelength ratio follows equation (35).

Introducing equations (35) and (38) into equation (46), the maximum charge per bunch becomes:

$$N_b \propto \omega^{-11/6}(a/\lambda)^{7/3} G_a^{2/3} \langle\beta_0\rangle^{-1/3} \propto \omega^{-5/3}(a/\lambda)^{13/6} G_a^{2/3} \propto \omega^{-37/30} G_a^{2/3} \tag{47}$$

Substituting for N_b in equation (34), the minimum possible bunch length becomes:

$$\sigma_z \propto \omega^{-5/6}(a/\lambda)^{1/3} G_a^{-1/3} \langle\beta_0\rangle^{-1/3} \propto \omega^{-2/3}(a/\lambda)^{1/6} G_a^{-1/3} \propto \omega^{-19/30} G_a^{-1/3} \tag{48}$$

As shown in Figs 10 and 11, the charge per bunch and the bunch length adopted in the TLC designs compare favourably with the above scaling laws:

Fig. 10: Variation of the charge per bunch in the TLC designs

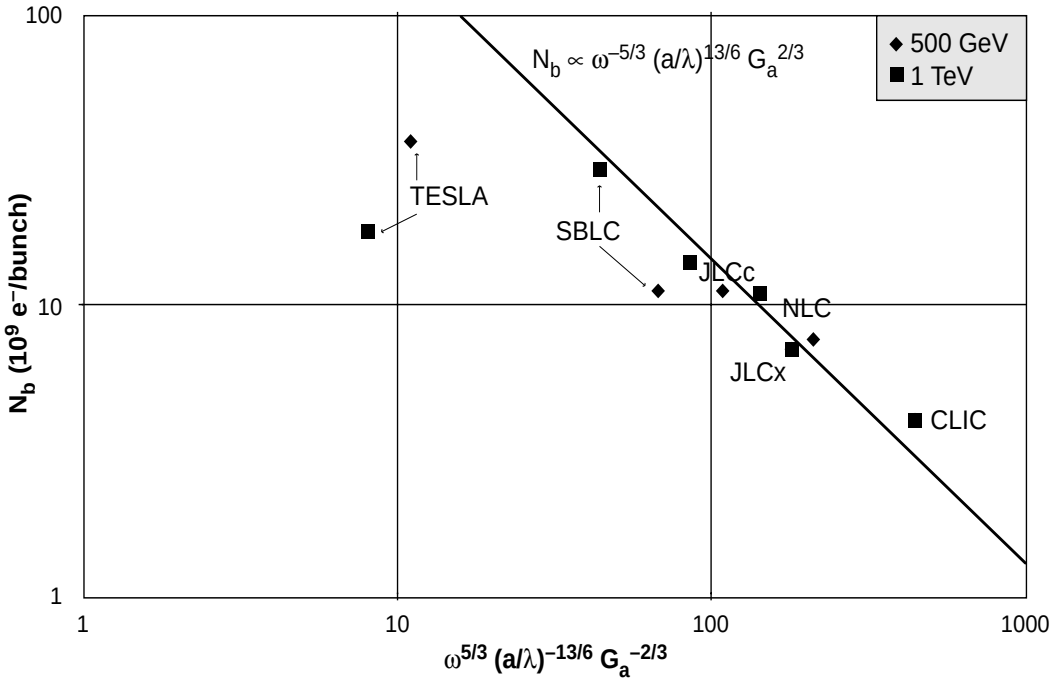

Fig. 11: Variation of the bunch length in the TLC designs

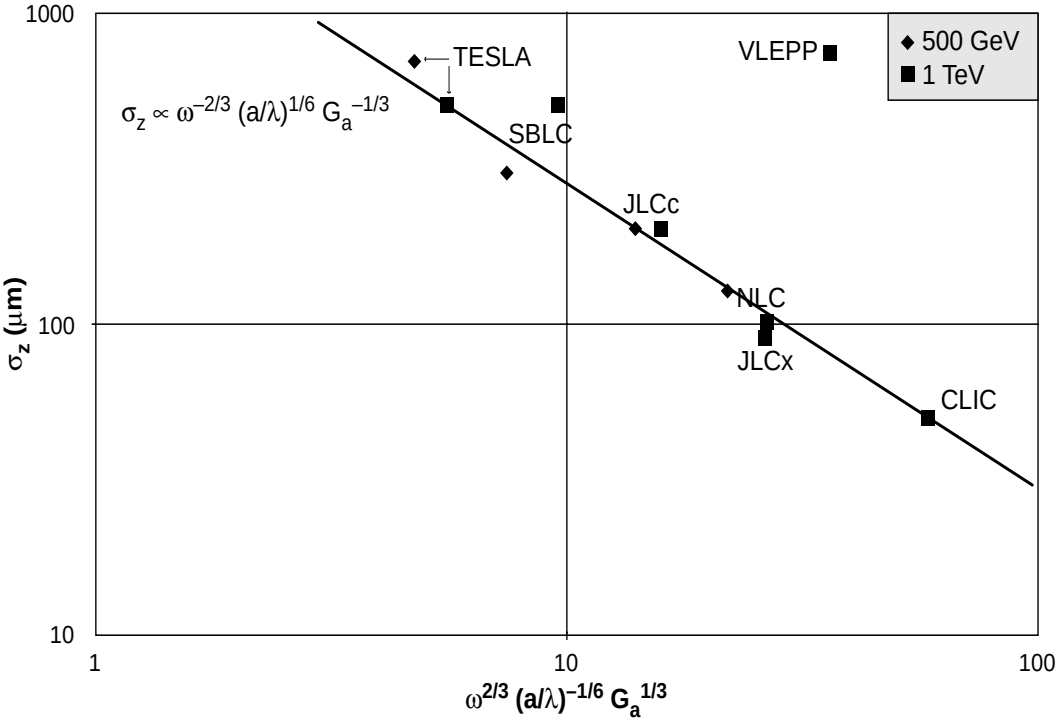

Similarly, introducing equations (46) and (47) into equations (26) and (45), the optimum length of the accelerating structures and the theoretical momentum spread for BNS damping become:

$$L_s = \frac{2Qv_g\tau_{opt}}{\omega} \propto \omega^{-7/6}(a/\lambda)^{5/3}G_a^{1/3}\langle\beta_0\rangle^{1/3} \propto \omega^{-4/3}(a/\lambda)^{11/6}G_a^{1/3} \propto \omega^{-29/30}G_a^{1/3} \quad (49)$$

$$\delta_{BNS} \propto \omega^{4/3}(a/\lambda)^{-5/6}G_a^{1/3}\langle\beta_0\rangle^{4/3} \propto \omega^{2/3}(a/\lambda)^{-1/6}G_a^{1/3} \propto \omega^{19/30}G_a^{1/3} \quad (50)$$

As shown in Figs 12 and 13 respectively, the structure lengths adopted for the various TLC designs and the δ_{BNS} calculated from the TLC parameters compare very reasonably with the above scaling laws:

Fig.12: Length of the accelerating structures in the TLC designs

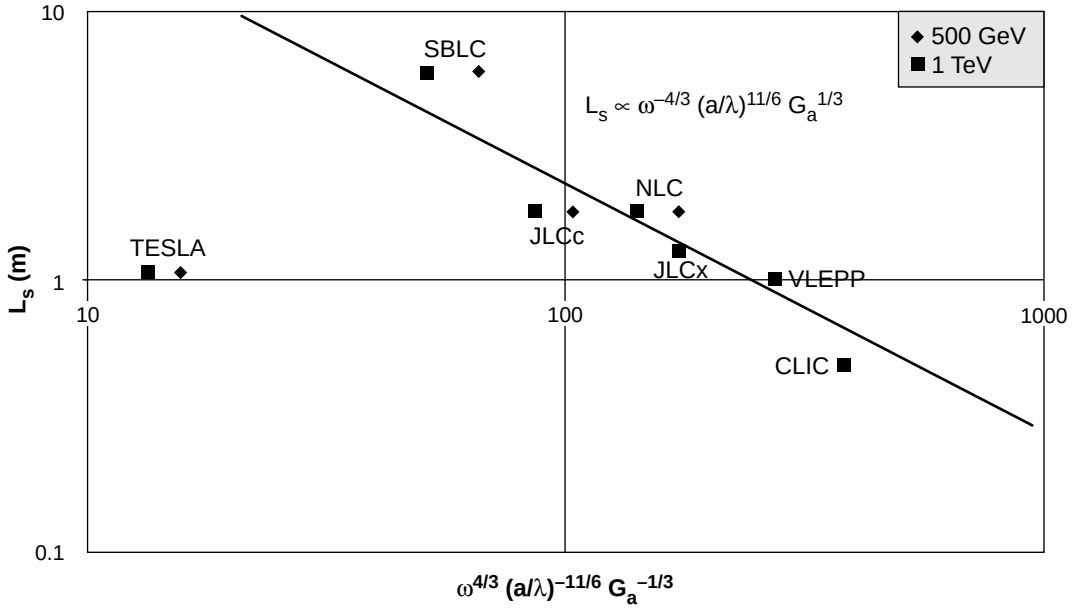

The BPM pre-alignment tolerance is deduced from the corresponding blow-up given by equation (30), introducing δ_{BNS} from equation (50) and taking into account of the condition imposed by equation (31):

$$(\Delta y_{BPM}) \propto \omega^{-4/3}(a/\lambda)^{5/6}G_a^{1/6}\langle\beta_0\rangle^{-1/3} \propto \omega^{-7/6}(a/\lambda)^{2/3}G_a^{1/6} \propto \omega^{-31/30}G_a^{1/6} \quad (51)$$

The scaling laws for the alignment tolerances of the RF structures (equation 39) and of the BPM (equation 51) are therefore very similar, with a weak dependence on the frequency and accelerating field:

$$(\Delta y_{BPM}) \propto \omega^{-1/4}G_a^{1/6}(\Delta y_{RF}) \quad (52)$$

Fig. 13: Theoretical momentum spread for BNS damping

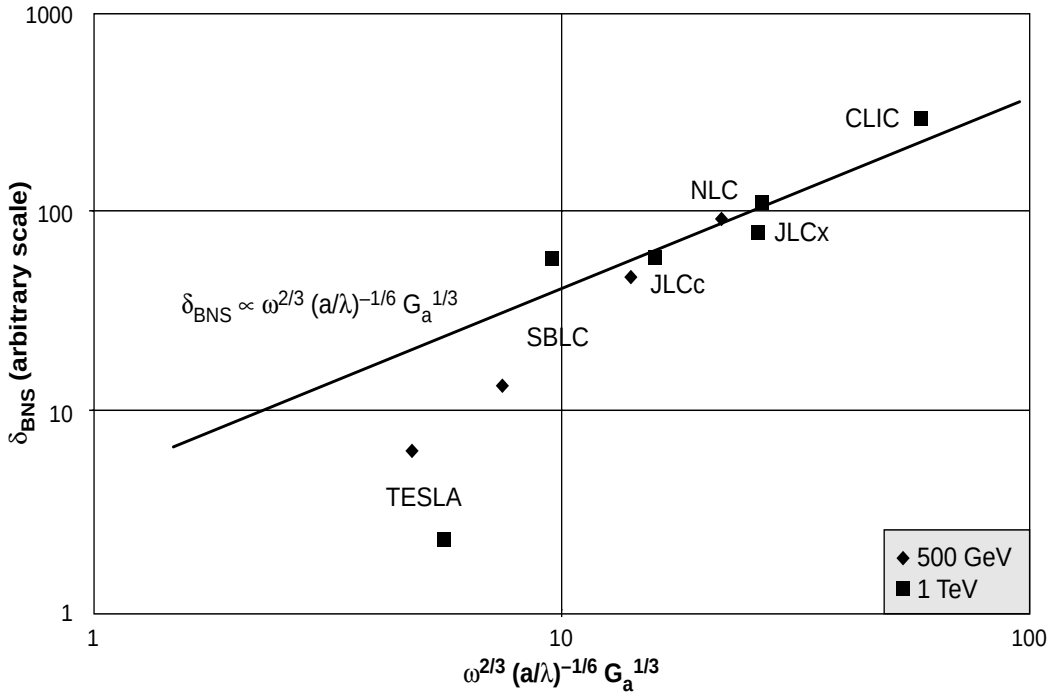

The strong dependence of the vertical blow-up induced by transverse wake fields on frequency as observed in equations (29) and (30) is therefore cancelled by an appropriate choice of the other parameters such that the blow-up is reduced to an acceptable level (a few tens of percent) for all TLC designs independently of the RF frequency:

$$\varepsilon_{ny}^{*} \propto \varepsilon_{ny} = \varepsilon_{nyo} + \Delta\varepsilon_{ny} \quad \text{with} \quad \Delta\varepsilon_{ny} \quad \text{independent of} \quad \omega \quad \text{and} \quad G_a \qquad (53)$$

Finally, by introducing the frequency dependence of the charge per bunch (equation 47) into equations (14) and (19), the normalised beam current and the RF to beam efficiency become roughly independent of the RF frequency and accelerating gradient (Fig. 14):

$$J \propto \omega^{-1/3}\left(a/\lambda\right)^{4/3} G_a^{-1/3} \left\langle \beta_0 \right\rangle^{-1/3} \propto \omega^{-1/6}\left(a/\lambda\right)^{7/6} G_a^{-1/3} \propto \omega^{1/15} G_a^{-1/3} \qquad (54)$$

$$\boxed{\eta_b^{RF} \propto J^{1/2} \propto \omega^{-1/6}\left(a/\lambda\right)^{2/3} G_a^{-1/6} \left\langle \beta_0 \right\rangle^{-1/6} \propto \omega^{-1/12}\left(a/\lambda\right)^{7/12} G_a^{-1/6} \propto \omega^{1/30} G_a^{-1/6}} \qquad (55)$$

Fig. 14: Normalized beam current in the TLC designs

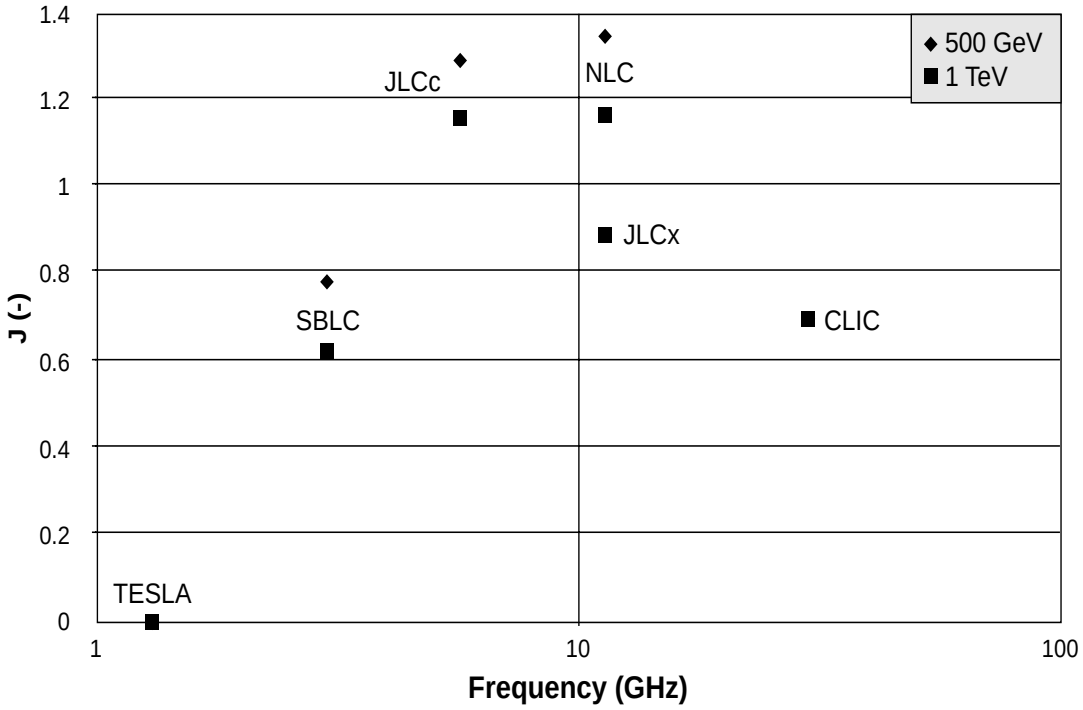

It can be seen that, in this case, increasing the accelerating gradient does not lead to the usual linear reduction of RF to beam efficiency because the charge per bunch can also be increased to obtain the same beam stability condition. Although the charge per bunch is reduced at high frequency, the RF to beam efficiency is nearly independent of the frequency because of the shorter interval between bunches, the larger iris to wavelength ratio and the increase of the shunt impedance with frequency.

In the low beamstrahlung regime, by intoducing equations (53) and (55) into equations (5) and (15), the figure of merit and corresponding luminosity also become roughly independent of the choice of RF frequency and of accelerating gradient:

$$M = L\frac{U_f}{\delta_B^{1/2}P_{AC}} \propto \frac{\eta_{beam}^{RF}}{\varepsilon_{ny}^{*1/2}} \propto \frac{\omega^{1/30}G_a^{-1/6}}{\left(\varepsilon_{nyo}+\Delta\varepsilon_{ny}\right)^{1/2}} \tag{56}$$

$$\boxed{L \propto \frac{\delta_B^{1/2}\eta_{RF}^{AC}}{U_f}\frac{\eta_{beam}^{RF}}{\varepsilon_{ny}^{*1/2}}P_{AC} \propto \frac{\delta_B^{1/2}\eta_{RF}^{AC}}{U_f}\frac{\omega^{1/30}G_a^{-1/6}}{\left(\varepsilon_{nyo}+\Delta\varepsilon_{ny}\right)^{1/2}}P_{AC}} \tag{57}$$

7. Beam sensitivity to ground motion and vibration tolerances

Because of ground motion, the alignment of the linac elements deteriorates with time. The ATL model [10] assumes that the correlation of the mean square of the relative transverse displacements between two points of the linac increases linearly with the time, T, and with the distance, L, between the two points. The coefficient, A, is a measure of the ground stability.

$$\left\langle \Delta X^2 \right\rangle = ATL \tag{58}$$

Although the ground motion affects the alignment of both the focusing elements and the accelerating structures, the beam trajectory can be maintained in place with beam-based correction trajectory techniques. Assuming, in an ideal case, a beam trajectory perfectly aligned along a straight line all along the linac, the beam emittance growth due to ground motion after a time, T, is only due to the drift in the transverse alignment of the accelerating structures and is given by [11]:

$$\Delta\varepsilon_{nACC} \propto AT \frac{N_b^2 \left\langle W_T^2 \right\rangle \left\langle \beta_0 \right\rangle^3 U_f^{11/4}}{G_a^2 U_o^{7/4} L_{Linac}} \tag{59}$$

where $\left\langle W_T^2 \right\rangle$ is the mean square average of the short range transverse wake field over the bunch.

Allowing a relative blow-up, $\left(\Delta\varepsilon_{ny} / \varepsilon_{ny}\right)_{ATL}$, of the beam emittance due to this effect in the vertical plane which is the most critical, the so-called "stable time", T_{ACC}, is the interval of time before a realignment of the linac elements or a beam trajectory correction has to be performed. Replacing the short range transverse wake, $\left\langle W_T \right\rangle$, by its expression (equation 25), and approximating the linac length, $L_{Linac} \propto U_f / G_a$, the stable time becomes:

$$T_{ACC} \propto \frac{G_a \varepsilon_{ny}}{A N_b^2 \sigma_z^2 \omega^8 (a/\lambda)^{-7} \left\langle \beta_0 \right\rangle^3} \left(\frac{U_0}{U_f}\right)^{7/4} \left(\frac{\Delta\varepsilon_{ny}}{\varepsilon_{ny}}\right)_{ATL}$$

$$T_{ACC} \propto \frac{G_a \left\langle \beta_0 \right\rangle \varepsilon_{ny}}{A \delta_{BNS}^2} \left(\frac{U_0}{U_f}\right)^{7/4} \left(\frac{\Delta\varepsilon_{ny}}{\varepsilon_{ny}}\right)_{ATL} \tag{60}$$

Assuming beam and linac parameters following the scaling laws described by equations (35), (38) and (50), the stable time, T_{ACC}, becomes:

$$\boxed{T_{ACC} \propto \frac{(a/\lambda)^{5/6} G_a^{1/3} \varepsilon_{ny}}{A\omega^{11/6}} \left(\frac{U_0}{U_f}\right)^{7/4} \left(\frac{\Delta\varepsilon_{ny}}{\varepsilon_{ny}}\right)_{ATL} \propto \frac{G_a^{1/3} \varepsilon_{ny}}{A\omega^{5/3}} \left(\frac{U_0}{U_f}\right)^{7/4} \left(\frac{\Delta\varepsilon_{ny}}{\varepsilon_{ny}}\right)_{ATL}} \tag{61}$$

As mentioned above, the ground motion also affects the alignment of the quadrupoles and therefore the beam trajectory. If uncorrected, this will cause an emittance dilution [8,12] after a time, T, of:

$$\Delta\varepsilon_{nQUAD} \propto ATN_{cell}^{3}\delta_{BNS}^{2} \tag{62}$$

where $N_{cell} \propto U_b/(G_a L_{cell})$ is the number of optics cells of length L_{cell}. In this case, the interval of time before the beam trajectory or the quadrupoles have to be realigned, the so-called "stable time", T_{QUAD}, is given by:

$$T_{QUAD} \propto \frac{G_a^3 L_{cell}^3 \varepsilon_{ny}}{A\delta_{BNS}^2}\left(\frac{U_o}{U_f}\right)^{3\alpha}\left(\frac{\Delta\varepsilon_{ny}}{\varepsilon_{ny}}\right)_{ATL} \tag{63}$$

Again, if the beam and linac parameters are chosen following the scaling laws of equations (35) and (38) , the stable time, T_{QUAD}, becomes:

$$\boxed{T_{QUAD} \propto \frac{G_a^{7/3}(a/\lambda)^{11/6}\varepsilon_{ny}}{A\omega^{17/6}}\left(\frac{U_o}{U_f}\right)^{3\alpha}\left(\frac{\Delta\varepsilon_{ny}}{\varepsilon_{ny}}\right)_{ATL} \propto \frac{G_a^{7/3}\varepsilon_{ny}}{A\omega^{37/15}}\left(\frac{U_o}{U_f}\right)^{3\alpha}\left(\frac{\Delta\varepsilon_{ny}}{\varepsilon_{ny}}\right)_{ATL}} \tag{64}$$

Equation (60) has been used to calculate the time for a relative emittance blow-up of 20% due to ground motion of the accelerating structures assuming an ATL model ($A = 1nm^2/m/s$) for the various TLC designs using the most up-to-date parameters (Tables 1 and 2). On the one hand, as shown in Fig.15, the corresponding stable times are decreasing with frequency by a factor of two over a range of frequencies covering one decade. On the other hand, the stable time due to the misalignment by ground motion of the quadrupoles is seen to increase with frequency because of the associated increase of accelerating gradient with frequency (Fig.16).

The effect of quadrupole jitter can be estimated and scaled in a similar manner. Here, high frequency vibration of the quadrupole magnets, $\langle y_{QUAD}\rangle$ induces beam jitter that cannot be corrected by the beam-based feedback systems. In units of the beam size, the induced beam jitter is [8]:

$$\frac{\langle \Delta y^2\rangle}{\sigma_y^2} \approx \langle y_{QUAD}^2\rangle \frac{4U_0 N_{CELL}}{\varepsilon_{ny} L_{oCELL}}\left(\frac{U_f}{U_o}\right)^{(1-\alpha)} \tan\left(\frac{\Psi}{2}\right) \tag{65}$$

where $\langle y_{QUAD}^2\rangle$ is the quadrupole vibration.

Rewriting equation (65) assuming a focusing optics along the linac following equation (38), an iris to wavelength ratio according to equation (35) and a constant phase advance per cell:

$$\left\langle y_{QUAD}^2 \right\rangle \propto \frac{\left\langle \Delta y^2 \right\rangle}{\sigma_y^2} \frac{G_a L_{0CELL}^2 \varepsilon_{ny}}{U_0^2} \left(\frac{U_0}{U_f} \right)^{2(1-\alpha)} \propto \frac{\left\langle \Delta y^2 \right\rangle}{\sigma_y^2} \frac{G_a}{\omega^{2/3}} \frac{\varepsilon_{ny}}{U_0^2} \left(\frac{U_0}{U_f} \right)^{2(1-\alpha)} \quad (66)$$

Again, if the gradient is scaled with the RF frequency as observed on Fig. 16, the vibration tolerance is found to be nearly independent of the frequency.

Fig. 15: Time stability in the TLC designs for a 20% blow-up due to ground motion

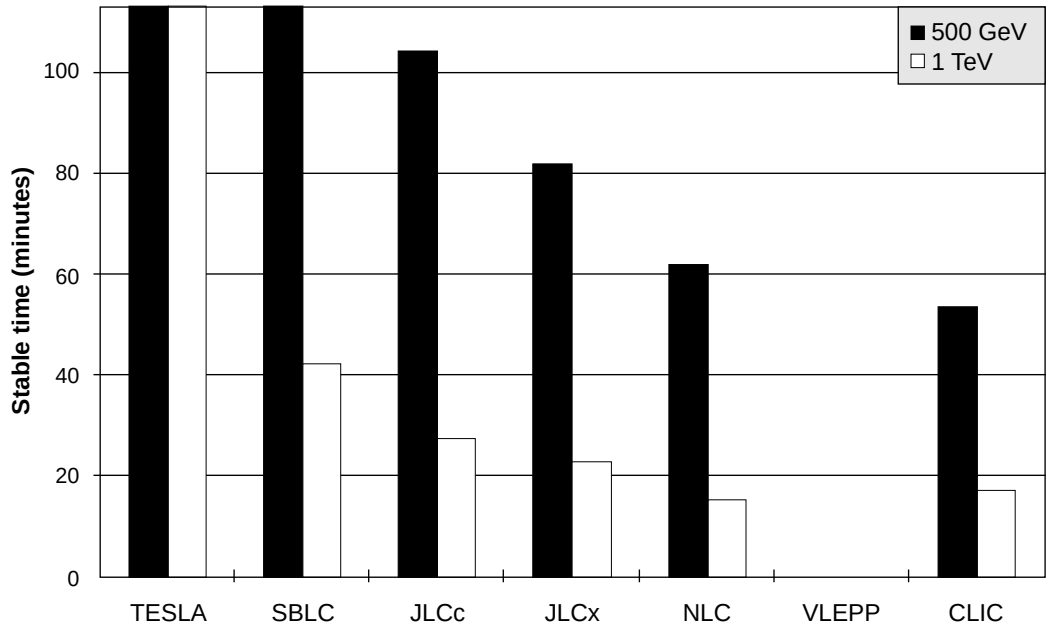

Fig. 16: Loaded accelerating gradients in the TLC designs

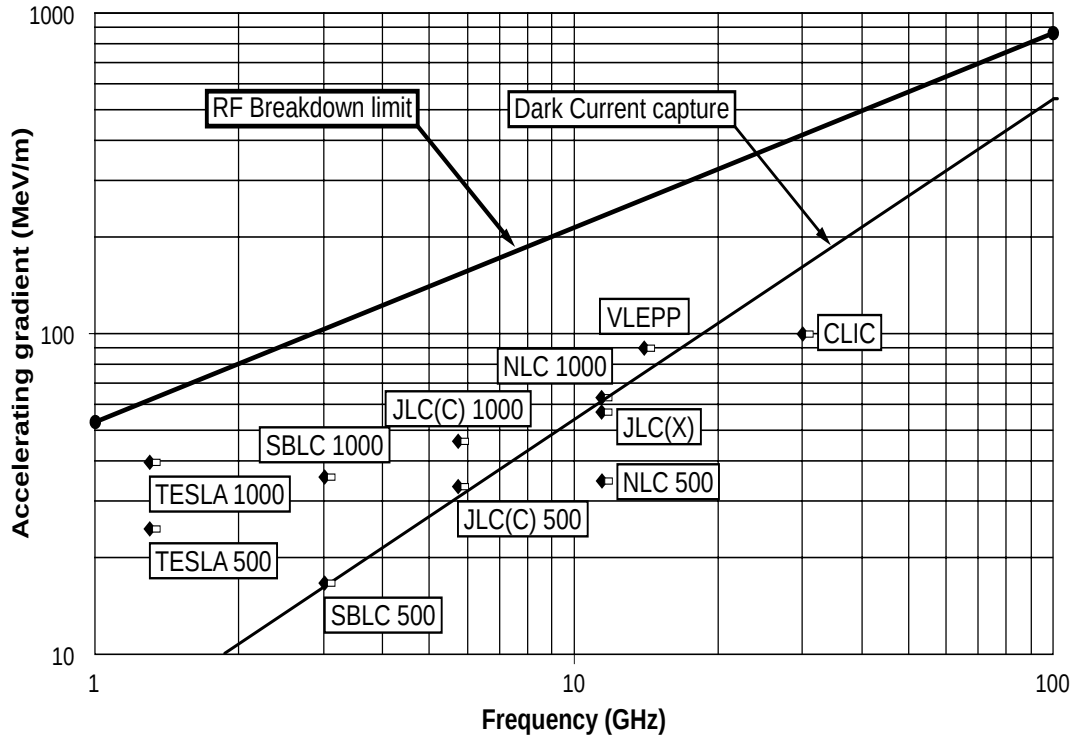

In many ways, these results are counter intuitive; a higher frequency providing as stable a beam as a low frequency one with a reduced sensitivity to component drifts. The explanation is that the jitter and ATL effects are strongly dependent on the number of focusing cells in the linac and, since higher frequencies enable higher accelerating gradients to be used, the length of the linac and therefore the number of cells can be significantly reduced.

8. Case of the high beamstrahlung regime

Very high energy Linear Colliders (E > 3 TeV) will certainly operate in the high beamstralung regime, Y >> 1 [13]. In this case, the luminosity is given by (equation A2-24):

$$L \propto \frac{\delta_B^{3/2}}{U_f^{1/2}} \frac{P_b}{\overline{\sigma}_y^* \sigma_z^{1/2}} \propto \frac{\delta_B^{3/2}}{U_f^{1/2}} \frac{\eta_b^{RF} \eta_{RF}^{AC} P_{AC}}{\sigma_z^{1/2} \beta_y^{*1/2} \varepsilon_{ny}^{*1/2}} \tag{67}$$

and the figure of merit is defined as:

$$M = \frac{L}{\delta_B^{3/2}} \frac{U_f^{1/2}}{P_{AC}} = \frac{\eta_{RF}^{AC}}{\beta_y^{*1/2}} \frac{\eta_b^{RF}}{\sigma_z^{1/2} \varepsilon_{ny}^{*1/2}} \propto \frac{\eta_b^{RF}}{\sigma_z^{1/2} \varepsilon_{ny}^{*1/2}} \tag{68}$$

when assuming equivalent AC to RF transfer efficiencies and focusing at the I.P.

Introducing equations (48), (53) and (55) in (68), the figure of merit and the luminosity scaling of a TLC equipped with a focusing optics along the linac following equation (38) becomes very favourable for high frequency – high gradient designs mainly due to the shorter bunch length:

$$M = \frac{L}{\delta_B^{3/2}} \frac{U_f^{1/2}}{P_{AC}} \propto \frac{\omega^{1/4} (a/\lambda)^{1/2}}{\varepsilon_{ny}^{1/2}} \propto \frac{\omega^{7/20}}{\varepsilon_{nyo}^{1/2} \left(1 + \Delta\varepsilon_{ny} / \varepsilon_{nyo}\right)^{1/2}} \tag{69}$$

$$\boxed{L \propto \frac{\delta_B^{3/2}}{U_f^{1/2}} \frac{\eta_{RF}^{AC}}{\beta_y^{*1/2}} \frac{\eta_b^{RF}}{\sigma_z^{1/2} \varepsilon_{ny}^{*1/2}} P_{AC} \propto \frac{\delta_B^{3/2}}{U_f^{1/2}} \frac{\eta_{RF}^{AC}}{\beta_y^{*1/2}} \frac{\omega^{7/20}}{\varepsilon_{nyo}^{1/2} \left(1 + \Delta\varepsilon_{ny} / \varepsilon_{nyo}\right)^{1/2}} P_{AC}} \tag{70}$$

However, it should be noted that practical considerations may limit the minimum bunch length attained in a collider. In this case, some of the benefits of the higher frquencies would not be realised [13].

9. Upgrade in energy and/or luminosity

An upgrade in luminosity can only be obtained either by raising the wall plug power and/or by reducing the initial vertical beam emittance and/or by increasing the δ_B parameter according to equations (57) and (70) in the low and high beamstrahlung regimes respectively.

When upgrading a linear collider in energy, the designed luminosity is further increased, if possible proportionally to the square of the C.o.M. energy, in order to keep the cross-section of the particle interactions during collisions, constant:

$$L \propto U_f^2 \tag{71}$$

The wall plug power is therefore a strong function of beam energy when providing a luminosity following equation (71):

In the low beamstrahlung regime: $$P_{AC} \propto \frac{U_f^3}{\delta_B^{1/2}\eta_{RF}^{AC}} \frac{\varepsilon_{nyo}^{1/2}\left(1+\Delta\varepsilon_{ny}/\varepsilon_{nyo}\right)^{1/2}}{\omega^{1/30}G_a^{-1/6}} \tag{72}$$

In the high beamstrahlung regime: $$P_{AC} \propto \frac{U_f^{5/2}}{\delta_B^{3/2}} \frac{\beta_y^{*1/2}}{\eta_{RF}^{AC}} \frac{\varepsilon_{nyo}^{1/2}\left(1+\Delta\varepsilon_{ny}/\varepsilon_{nyo}\right)^{1/2}}{\omega^{7/20}} \tag{73}$$

This is the reason why, in order to limit the wall plug power, the initial vertical beam emittance, ε_{nyo} is reduced as much as possible and, in very high energy linear colliders [13], the δ_B parameter is allowed to increase (moving into high beamstrahlung regime which is acceptable by physics conditions at high energy).

For very small vertical beam emittances, the hypothesis of a constant absolute value of the transverse blow-up (equation 31), that has been assumed in this paper for the scaling of the parameters and that is presently adopted in the various TLC designs, is not sufficient as it would make the performance of the collider predominantly dependent on the vertical blow-up. When upgrading a given design in energy and/or luminosity, the relative rather than the absolute transverse blow-up should be kept constant:

$$\frac{\Delta\varepsilon_{ny}}{\varepsilon_{nyo}} = Const. \tag{74}$$

In this case, the exact same scaling strategy can be adopted except that equation (31) is replaced by equation (74). The charge which produces a tolerable beam blow-up induced by the misalignment of the RF structures according to condition (74) is deduced by substituting the relations found above for the scaling of the different parameters (equations 34, 35, 38, 39 and 45) into equation (29):

$$N_b \propto \omega^{-11/6}\left(a/\lambda\right)^{7/3} G_a^{2/3}\left\langle\beta_o\right\rangle^{-1/3}\varepsilon_{nyo}^{1/3} \propto \omega^{-5/3}\left(a/\lambda\right)^{13/6} G_a^{2/3}\varepsilon_{nyo}^{1/3}$$

$$N_b \propto \omega^{-37/30} G_a^{2/3}\varepsilon_{nyo}^{1/3} \tag{75}$$

Not surprisingly, the scaling law is the same as the one found previously (equation 47) with an additional dependency on initial beam emittance.

Substituting for N_b respectively in equations (34), (26), (45), (50), (60), (63), (65), (14) and (19), the minimum possible bunch length, the optimum length of the accelerating structure, the theoretical momentum spread for BNS damping, the BPM pre-alignment tolerance, the stable times with ground motion, the vibration tolerance, the normalised beam current and the RF to beam efficiency become:

$$\sigma_z \propto \omega^{-5/6}\left(a/\lambda\right)^{1/3} G_a^{-1/3}\left\langle\beta_o\right\rangle^{-1/3}\varepsilon_{nyo}^{1/3} \propto \omega^{-2/3}\left(a/\lambda\right)^{1/6} G_a^{-1/3}\varepsilon_{nyo}^{1/3}$$

$$\sigma_z \propto \omega^{-19/30} G_a^{-1/3}\varepsilon_{nyo}^{1/3} \tag{76}$$

$$L_s \propto \omega^{-7/6}\left(a/\lambda\right)^{5/3} G_a^{1/3}\left\langle\beta_o\right\rangle^{1/3}\varepsilon_{ny0}^{-1/3} \propto \omega^{-4/3}\left(a/\lambda\right)^{11/6} G_a^{1/3}\varepsilon_{ny0}^{-1/3}$$

$$L_s \propto \omega^{-29/30} G_a^{1/3}\varepsilon_{ny0}^{-1/3} \tag{77}$$

$$\delta_{BNS} \propto \omega^{4/3}\left(a/\lambda\right)^{-5/6} G_a^{1/3}\left\langle\beta_o\right\rangle^{4/3}\varepsilon_{nyo}^{2/3} \propto \omega^{2/3}\left(a/\lambda\right)^{-1/6} G_a^{1/3}\varepsilon_{nyo}^{2/3}$$

$$\delta_{BNS} \propto \omega^{19/30} G_a^{1/3}\varepsilon_{nyo}^{2/3} \tag{78}$$

$$\left(\Delta y_{BPM}\right) \propto \omega^{-4/3}\left(a/\lambda\right)^{5/6} G_a^{1/6}\left\langle\beta_o\right\rangle^{-1/3}\varepsilon_{nyo}^{7/6} \propto \omega^{-7/6}\left(a/\lambda\right)^{2/3} G_a^{1/6}\varepsilon_{nyo}^{7/6}$$

$$\left(\Delta y_{BPM}\right) \propto \omega^{-31/30} G_a^{1/6}\varepsilon_{nyo}^{7/6} \tag{79}$$

$$T_{ACC} \propto \frac{\left(a/\lambda\right)^{5/6} G_a^{1/3}}{A\omega^{11/6}\varepsilon_{nyo}^{1/3}}\left(\frac{U_0}{U_f}\right)^{7/4}\left(\frac{\Delta\varepsilon_{ny}}{\varepsilon_{ny}}\right)_{ATL} \propto \frac{G_a^{1/3}}{A\omega^{5/3}\varepsilon_{nyo}^{1/3}}\left(\frac{U_0}{U_f}\right)^{7/4}\left(\frac{\Delta\varepsilon_{ny}}{\varepsilon_{ny}}\right)_{ATL} \tag{80}$$

$$T_{QUAD} \propto \frac{G_a^{7/3}\left(a/\lambda\right)^{11/6}}{A\omega^{17/6}\varepsilon_{nyo}^{1/3}}\left(\frac{U_o}{U_f}\right)^{3\alpha}\left(\frac{\Delta\varepsilon_{ny}}{\varepsilon_{ny}}\right)_{ATL} \propto \frac{G_a^{7/3}}{A\omega^{37/15}\varepsilon_{nyo}^{1/3}}\left(\frac{U_o}{U_f}\right)^{3\alpha}\left(\frac{\Delta\varepsilon_{ny}}{\varepsilon_{ny}}\right)_{ATL} \tag{81}$$

$$\left\langle y_{QUAD}^2 \right\rangle \propto \frac{\left\langle \Delta y^2 \right\rangle}{\sigma_y^2} \frac{G_a L_{0CELL}^2 \varepsilon_{nyo}}{U_0^2} \left(\frac{U_0}{U_f} \right)^{2(1-\alpha)} \propto \frac{\left\langle \Delta y^2 \right\rangle}{\sigma_y^2} \frac{G_a}{\omega^{4/5}} \frac{\varepsilon_{nyo}}{U_0^2} \left(\frac{U_0}{U_f} \right)^{2(1-\alpha)} \tag{82}$$

$$J \propto \omega^{-1/3} \left(a/\lambda \right)^{4/3} G_a^{-1/3} \left\langle \beta_o \right\rangle^{-1/3} \varepsilon_{nyo}^{1/3} \propto \omega^{-1/6} \left(a/\lambda \right)^{7/6} G_a^{-1/3} \varepsilon_{nyo}^{1/3}$$

$$J \propto \omega^{1/15} G_a^{-1/3} \varepsilon_{nyo}^{1/3} \tag{83}$$

$$\eta_b^{RF} \propto J^{1/2} \propto \omega^{-1/6} \left(a/\lambda \right)^{2/3} G_a^{-1/6} \left\langle \beta_o \right\rangle^{-1/6} \varepsilon_{nyo}^{1/6} \propto \omega^{-1/12} \left(a/\lambda \right)^{7/12} G_a^{-1/6} \varepsilon_{nyo}^{1/6}$$

$$\eta_b^{RF} \propto \omega^{1/30} G_a^{-1/6} \varepsilon_{nyo}^{1/6} \tag{84}$$

Finally introducing equation (55) into equations (5), (15), (68), and (70), the figure of merit, the luminosity and the wall plug power for a luminosity scaling with the square of the energy, become respectively:

in the low beamstrahlung regime:

$$M = L \frac{U_f}{\delta_B^{1/2} P_{AC}} \propto \frac{\eta_{beam}^{RF}}{\varepsilon_{ny}^{*1/2}} \propto \frac{\omega^{1/30} G_a^{-1/6}}{\varepsilon_{nyo}^{1/3} \left(1 + \Delta\varepsilon_{ny} / \varepsilon_{nyo} \right)^{1/2}} \tag{85}$$

$$L \propto \frac{\delta_B^{1/2} \eta_{RF}^{AC}}{U_f} \frac{\eta_{beam}^{RF}}{\varepsilon_{ny}^{*1/2}} P_{AC} \propto \frac{\delta_B^{1/2} \eta_{RF}^{AC}}{U_f} \frac{\omega^{1/30} G_a^{-1/6}}{\varepsilon_{nyo}^{1/3} \left(1 + \Delta\varepsilon_{ny} / \varepsilon_{nyo} \right)^{1/2}} P_{AC} \tag{86}$$

$$P_{AC} \propto \frac{U_f^3}{\delta_B^{1/2} \eta_{RF}^{AC}} \frac{\varepsilon_{nyo}^{1/3} \left(1 + \Delta\varepsilon_{ny} / \varepsilon_{nyo} \right)^{1/2}}{\omega^{1/30} G_a^{-1/6}} \tag{87}$$

in the high beamstrahlung regime:

$$M = \frac{L}{\delta_B^{3/2}} \frac{U_f^{1/2}}{P_{AC}} \propto \frac{\omega^{1/4} \left(a/\lambda \right)^{1/2}}{\varepsilon_{ny}^{*1/2}} \propto \frac{\omega^{7/20}}{\varepsilon_{ny}^{1/2} \left(1 + \Delta\varepsilon_{ny} / \varepsilon_{nyo} \right)^{1/2}} \tag{88}$$

$$L \propto \frac{\delta_B^{3/2}}{U_f^{1/2}} \frac{\eta_{RF}^{AC}}{\beta_y^{*1/2}} \frac{\eta_b^{RF}}{\sigma_z^{1/2} \varepsilon_{ny}^{*1/2}} P_{AC} \propto \frac{\delta_B^{3/2}}{U_f^{1/2}} \frac{\eta_{RF}^{AC}}{\beta_y^{*1/2}} \frac{\omega^{7/20}}{\varepsilon_{ny}^{1/2} \left(1 + \Delta\varepsilon_{ny} / \varepsilon_{nyo} \right)^{1/2}} P_{AC} \tag{89}$$

$$P_{AC} \propto \frac{U_f^{5/2}}{\delta_B^{3/2}} \frac{\beta_y^{*1/2}}{\eta_{RF}^{AC}} \frac{\varepsilon_{ny}^{1/2} \left(1 + \Delta\varepsilon_{ny} / \varepsilon_{nyo} \right)^{1/2}}{\omega^{7/20}} \tag{90}$$

10. Conclusion

A figure of merit, defined for the same colliding beam energy, as the luminosity normalised to both the beamstrahlung parameter and to the wall plug power consumption, has been used to optimise the design of a future TeV e^+e^- Linear Collider. ***This figure of merit is dependent only on two parameters: the AC to beam power transfer efficiency and the vertical beam emittance at the interaction point.*** The design process consists of selecting appropriate linac and beam parameters to optimise these two parameters.

General scaling laws have been derived for both the linac and the beam parameters with an infinite number of bunches for stable beam operation and for minimisation of the energy spread at the end of the linac. Under these conditions, the main beam parameters (bunch charge and bunch length) are fully determined (equations 75 and 76 after rounding off the exponents):

$$N_b \propto \omega^{-6/5} G_a^{2/3} \varepsilon_{nyo}^{1/3} \qquad \text{and} \qquad \sigma_z \propto \omega^{-2/3} G_a^{-1/3} \varepsilon_{nyo}^{1/3}$$

Using these beam parameters and choosing the following optimum field attenuation for the RF structures to obtain an optimum RF to beam efficiency (equations A3-22, 54 and 83) for small values of the beam loading parameter:

$$\tau_{opt} \propto J^{-1} \propto \omega^{-1/15} G_a^{1/3} \varepsilon_{nyo}^{-1/3}$$

it is found that (again after rounding off the exponents):

- ***The RF to beam efficiency is nearly independent of accelerating gradient and RF frequency*** (equations 55 and 84), in the range of parameters considered by the various TLC designs:

$$\eta_b^{RF} \propto J^{1/2} \propto \omega^{1/30} G_a^{-1/6} \varepsilon_{nyo}^{1/6}$$

- In spite of the large increase in the wake-fields induced by the accelerating structures with increasing frequency, ***the effect of the wake-fields, and the corresponding beam emittance blow-up for equivalent beam trajectory correction techniques, is made independent of the frequency*** (equation 31) because both the charge per bunch and the bunch length are substantially reduced (equations 47 and 48). This is obtained at the expense of:
  - A stronger focusing optics along the linac (equation 38)

$$\langle \beta_o \rangle \propto (a/\lambda)^{1/2} \omega^{-1/2} \propto \omega^{-2/5}$$

  - Tighter alignment tolerances of the RF structures and Beam Position Monitors, BPMs (equations 39, 51 and 79)

$$\langle \Delta y_{RF} \rangle \propto \omega^{-3/4} \qquad \text{and} \qquad (\Delta y_{BPM}) \propto \omega^{-1} G_a^{1/6} \varepsilon_{nyo}$$

- Larger momentum spread along the bunch for BNS damping (equation 78)

$$\delta_{BNS} \propto N_b \sigma_z \beta_o^2 \left(a/\lambda\right)^{-7/2} \omega^4 \propto \omega^{2/3} G_a^{1/3} \varepsilon_{nyo}^{2/3}$$

- ***In the low beamstrahlung regime*** which is generally adopted for intermediate energy TLC designs (0.5 to 2 TeV), ***the figure of merit and the luminosity increase slightly with RF frequency and decrease slightly with accelerating gradient*** (Equations 85 and 86):

$$M = L \frac{U_f}{\delta_B^{1/2} P_{AC}} \propto \frac{\eta_{beam}^{RF}}{\varepsilon_{ny}^{*1/2}} \propto \frac{\omega^{1/30} G_a^{-1/6}}{\varepsilon_{nyo}^{1/3} \left(1 + \Delta\varepsilon_{ny}/\varepsilon_{nyo}\right)^{1/2}}$$

$$\boxed{L \propto \frac{\delta_B^{1/2} \eta_{RF}^{AC}}{U_f} \frac{\eta_{beam}^{RF}}{\varepsilon_{ny}^{*1/2}} P_{AC} \propto \frac{\delta_B^{1/2} \eta_{RF}^{AC}}{U_f} \frac{\omega^{1/30} G_a^{-1/6}}{\varepsilon_{nyo}^{1/3} \left(1 + \Delta\varepsilon_{ny}/\varepsilon_{nyo}\right)^{1/2}} P_{AC}}$$

- ***In the high beamstrahlung regime*** which is usually adopted for high energy TLC designs (3 to 5 TeV), ***the figure of merit and therefore the luminosity increase with RF frequency but are independent of accelerating gradient*** (equations 88 and 89):

$$M = \frac{L}{\delta_B^{3/2}} \frac{U_f^{1/2}}{P_{AC}} \propto \frac{\eta_{RF}^{AC}}{\beta_y^{*1/2}} \frac{\eta_b^{RF}}{\sigma_z^{1/2} \varepsilon_{ny}^{*1/2}} \propto \frac{\eta_b^{RF}}{\sigma_z^{1/2} \varepsilon_{ny}^{*1/2}} \propto \frac{\omega^{1/3}}{\varepsilon_{nyo}^{1/2} \left(1 + \Delta\varepsilon_{ny}/\varepsilon_{nyo}\right)^{1/2}}$$

$$\boxed{L \propto \frac{\delta_B^{3/2}}{U_f^{1/2}} \frac{\eta_{RF}^{AC}}{\beta_y^{*1/2}} \frac{\eta_b^{RF}}{\sigma_z^{1/2} \varepsilon_{ny}^{*1/2}} P_{AC} \propto \frac{\delta_B^{3/2}}{U_f^{1/2}} \frac{\eta_{RF}^{AC}}{\beta_y^{*1/2}} \frac{\omega^{1/3}}{\varepsilon_{nyo}^{1/2} \left(1 + \Delta\varepsilon_{ny}/\varepsilon_{nyo}\right)^{1/2}} P_{AC}}$$

- ***The wall plug power consumption of a linear collider*** providing a luminosity which scales with the square of the C.o.M. energy for a constant cross-section of particle interactions, ***is a strong function of the beam energy*** (equations 87 and 90):

In the low beamstrahlung regime: $$P_{AC} \propto \frac{U_f^3}{\delta_B^{1/2} \eta_{RF}^{AC}} \frac{\varepsilon_{nyo}^{1/3} \left(1 + \Delta\varepsilon_{ny}/\varepsilon_{nyo}\right)^{1/2}}{\omega^{1/30} G_a^{-1/6}}$$

In the high beamstrahlung regime: $$P_{AC} \propto \frac{U_f^{5/2}}{\delta_B^{3/2}} \frac{\beta_y^{*1/2}}{\eta_{RF}^{AC}} \frac{\varepsilon_{nyo}^{1/2} \left(1 + \Delta\varepsilon_{ny}/\varepsilon_{nyo}\right)^{1/2}}{\omega^{7/20}}$$

In order to limit the wall plug power consumption, very high energy linear colliders will have to operate in the high beamstrahlung regime with extremely low vertical beam emittances.

- ***The scaling laws described in this paper are not unique.*** The set presented here in which the beam emittance dilution is assumed to be independent of frequency and the alignment tolerances of the RF components are assumed to vary as $\omega^{-3/4}$, provides a consistent method in the process of optimising a Linear Collider design. It closely reflects what is done in practice as demonstrated by the excellent agreement with the variation of parameters adopted in the various TLC designs. Other options leading to slightly different scaling laws have also been investigated, for example assuming both the beam emittance and the wall plug power to be independent of RF frequency. It was found however that the general tendency of the variation of the parameters and the main conclusions remain very similar.

Finally the use of high frequency accelerating structures for the main linacs of a future TeV e^+e^- Linear Collider is particularly appropriate since high frequencies allow operation with high accelerating gradients which minimise the overall length and therefore the cost of the linac. As long as the beam and linac parameters are chosen both to fulfil beam stability criteria and to minimise the final energy spread, and optimum structure parameters are selected to maximise the RF efficiency, then high frequency designs operating with high accelerating gradients result in the same or better RF efficiency and figure of merit, with a similar beam quality preservation for equivalent beam correction techniques as the lower frequency designs operating with lower accelerating gradients.

11. References

[1] International Linear Collider Technical Review Committee Report 1995, SLAC-R-95-471.
[2] P.Chen, “Disruption effects from the collision of quasi-flat beams”, Proc. Part. Acc. Conf. Washington, 1993 and SLAC-PUB-6215, April 1993.
[3] K.Yokoya and P.Chen, “Beam-Beam phenomena in linear colliders”, Frontiers of particle beams, Lecture notes in Physics 400, 1990.
[4] G.A.Loew and R.B.Neal: “Accelerating structures”, Part B, Section 1.1 p 39. Of Linear Accelerators edited by P.M.Lapostolle and A.Septier; North-Holland Publishing Company-Amsterdam 1970.
[5] V.E.Balakin, A.V.Novokhatsky, V.P.Smirnov, 12th Int. Conf. On High Energy Accelerators, Fermilab 1983, p119.
[6] T.O.Raubenheimer, “Generation and preservation of low emittance flat beams”, PhD thesis, Stanford University (1991) and G.Guignard, “Beam dynamics issues and the CLIC target parameters”, CLIC note 320.
[7] R.B.Palmer, “Prospects for High Energy e+/e- Linear Colliders”, Ann. Rev. Nucl. Part. Sci. 40: 529 (1990).
[8] T.O.Raubenheimer, “Summary of Formula for Emittance Dilution in High Energy Linacs”, CLIC Note 347 (1997)
[9] Z.D.Farkas, “The roles of frequency and aperture in linac accelerator design”, SLAC-PUB-4722, September 1988 and “Unified formulation for linear accelerator design”, SLAC-PUB-3981, May 1986.
[10] B.Baklakhov, P.Lebedev, V.Parkhomchuk, A.Sery, A.Sleptov and V.Shiltsev, INP 91-15; Tech. Ph.38,984, (1993).
[11] S.Takeda, N.Yamamoto and K.Oide, Particle Accelerator Conference in Vancouver, Canada (12-16 May 1997).
[12] A.Sery, O.Napoly, “Influence of Ground Motion on the Time Evolution of Beams in Linear Colliders”, Phys. Rev. E 53: 5323 (1996)
[13] J.P.Delahaye, G.Guignard, J.Irwin, T.O.Raubenheimer, R.D.Ruth, I.Wilson and P.B.Wilson, ”A 30 GHz - 5 TeV TLC design”, CERN/PS 97-23 (LP), CLIC Note 339 and 1997 Particle Accelerator Conference, 12-16.5.97, Vancouver, B.C., Canada.
[14] K.A. Thompson and R.D.Ruth, “Simulation and compensation of multibunch energy variation in 0.5 to 1.0 TeV Linear Collider designs”, SLAC-PUB-5882.
[15] R.P.Borghi, A.L.Eldridge and al., “Design, fabrication, installation and performance of the accelerator structure”, chapter 6, p95 of The Stanford Two-Mile Accelerator” edited by R.B.Neal, W.A Benjamin, Inc. New York Amsterdam (1968). and R.B.Neal, “Theory of the constant gradient linear electron accelerator”, Rept. No ML-513, Microwave Laboratory, Stanford University, Stanford (CA), (1958).

Table 1: TLC main parameters at 500 GeV (updated from [1])

Study	Unit	Symb	TESLA	SBLC	JLCc	JLCx	NLC	VLEPP	CLIC
Beam parameters at IP									
Luminosity (with pinch/no dil.)	$[10^{33}cm^{-2}sec^{-1}]$	L	6.0	5.3	7.18	6.11	6.8	9.7	6.25
Effect lumin. (with FF dilution)	$[10^{33}cm^{-2}sec^{-1}]$	L	6.0	5.3	7.18	6.11	5.5	9.7	5.0
Beamstrahlung mom. spread	[%]	δ_B	2.5	2.8	4.1	3.4	3.2	10	3.5
Beamsthralung parameter	[-]	Y	0.03	0.042	0.144	0.12	0.09	0.074	0.17
Number of photons/electron	[-]	n_γ	2.0	1.4	1.5	0.9	1.1	4.7	0.73
Linac repetition rate	[Hz]	f	5	50	100	150	180	300	511
Number of particles/bunch	$[10^9 e^{\pm}]$	N_b	36.3	11	11.1	7	7.5	200	4
Number of bunches/pulse	[-]	k_b	1130	333	72	85	90	1	60
Bunch spacing	[nsec]	Δ_b	708	6	2.8	1.4	1.4	-	0.67
Transverse emittances	$[10^{-8}$ radm]	$\gamma\varepsilon_{x/y}$	1400/25	500/25	330/5	330/5	400/9	2000/8	188/10
Beta functions	[mm]	$\beta_{x/y}$	25/0.7	11/0.45	15/0.2	10/0.1	10/0.15	100/0.1	10/0.10
RMS beam width (FF diluted)	[nm]	$\sigma^*_{x/y}$	845/19	335/15.1	260/3	260/3.1	294/6.3	2000/4	206/5.4
Bunch length	[μm]	σ_z	700	300	200	90	125	750	50
Enhancement factor	[-]	H_D	1.63	1.68	1.7	1.57	1.41	0.82	1.43
Beam power per beam	[MW]	P_b	8.2	7.25	3.07	3.57	4.8	2.4	4.91
Main Linac									
RF frequency of main linac	[GHz]	$\omega/2\pi$	1.3	3	5.7	11.4	11.4	14	30
Accelerating field (loaded)	[MV/m]	G	25/25	21/17	40/33	73/58.2	50/35	100/91	122/100
Total two linacs length	[km]	l_{tot}	30	32	18.8	10.5	17.6	7	7.5
Length of sections	[m]	ℓ_{sec}	1.04	6	1.8	1.31	1.8	1	0.49
Field attenuation per section	[-]	τ	-	0.55	0.53	0.58	0.53	0.79	0.675
<Normal. shunt impedance>	[kΩ/m]	r'	1.0	3.6-4.7	5.49	10.2-13.6	9.1-13.2	17.7	25.0
<Quality factor (Q_0 for SW)>	$[10^3]$	Q	3000	13.5	9.67	7.2-6.4	7.4-6.7	6.0	3.5
<Iris to RF wavelength ratio>	[-]	a/λ	0.15	0.16-0.11	0.173-0.125	0.20-0.14	0.22-0.15	0.14	0.20
Beam loading parameter	[%]	δ	0.0	19.0	17.5	20.3	30.0	9.0	18.2
Peak RF power at section input	[MWatts]	P_{sec}	0.213	73	84.3	130	150	120	112.5
RF pulse length	[μsec]	Δ_t	1315	2.80	0.485	0.230	0.240	0.110	0.065
RF pulse compression ratio	[-]	-	1	1	5	3	3.3	3.2	1
Total number of klystrons or drive	[-]	N_{kly}	616	2517	4184	4400	4528	1400	1-6
AC to RF efficiency	[%]	η^{Ac}	35	37	22.6	30	28	39	35
RF to beam efficiency	[%]	η^{RF}_{beam}	47.14	28.11	17.7	20	28.2	21.5	29.74
AC to beam efficiency	[%]	η^{AC}	16.5	10.4	4	6.0	7.9	8.4	10.4
AC power for RF generation	[MW]	P_{ac}	99	140	153	115	121	57	94.3
Figure of Merit	$10^{37}cm^{-2}s^{-1}A^{-1}$	M	9.5	5.6	5.5	7.0	7.7	13.4	8.8

Table 2: TLC main parameters at 1 TeV (updated from [1])

Study	Unit	Symb	TESLA	SBLC	JLCc	JLCx	NLC	VLEPP	CLIC
Beam parameters at IP									
Luminosity (with pinch/no dil.)	$[10^{33}cm^{-2}sec^{-1}]$	L	11	6.3	7.6	16.7	17.8	13	12.5
Effect lumin. (with FF dilution)	$[10^{33}cm^{-2}sec^{-1}]$	L	11	6.3	7.6	16.7	14.5	13	10.0
Beamstrahlung mom. spread	[%]	δ_B	2.2	6.5	8.3	9.9	7.4	26.6	10
Beamsthralung parameter	[-]	Y	0.05	0.06	0.29	0.33	0.27	0.15	0.54
Number of photons/electron	[-]	n_γ	1.2	1.4	1.73	1.43	1.1	5	1.03
Linac repetition rate	[Hz]	f	3	50	50	150	120	300	444
Number of particles/bunch	$[10^9 e^{\pm}]$	N_b	18	29	13.9	7	11	200	4
Number of bunches/pulse	[-]	k_b	2260	50	72	85	75	1	60
Bunch spacing	[nsec]	Δ_b	283	10	2.8	1.4	1.4	-	0.67
Transverse emittances	$[10^{-8}$ radm]	$\gamma\varepsilon_{x/y}$	1200/2.5	1000/10	330/5	330/5	500/5	2000/8	147/10
Beta functions	[mm]	$\beta_{x/y}$	25/0.5	32/0.8	30/0.2	10/0.1	25/0.1	200/0.1	10/0.10
RMS beam width (FF diluted)	[nm]	$\sigma^*_{x/y}$	618/4	572/9	318/3.14	184/2.3	360/2.3	2000/2.7	129/3.8
Bunch length	[μm]	σ_z	500	500	200	90	100	750	50
Enhancement factor	[-]	H_D	1.64	1.68	1.6	1.6	1.35	2	1.46
Beam power per beam	[MW]	P_b	9.75	5.8	4	7.15	7.9	4.8	8.53
Main Linac									
RF frequency of main linac	[GHz]	$\omega/2\pi$	1.3	3	5.7	11.4	11.4	14	30
Accelerating field (loaded)	[MV/m]	G	40/40	42/36	56/47	73/58	85/63	100/91	122/100
Total two linacs length	[km]	l_{tot}	37.5	33	26.6	21.8	18.7	14	15
Length of sections	[m]	ℓ_s	1.04	6	1.8	1.31	1.8	1	0.49
Field attenuation per section	[-]	τ	-	0.55	0.53	0.58	0.53	0.79	0.675
<Normal. shunt impedance>	[kΩ/m]	r'	1.0	3.6-4.7	5.49	10.2-13.6	9.1-13.2	17.7	25.0
<Quality factor (Q_0 for SW)>	$[10^3]$	Q	3000	13.5	9.67	7.2-6.4	7.4-6.7	6.0	3.5
<Iris to RF wavelength ratio>	[-]	a/λ	0.15	0.16-0.11	0.173-0.125	0.20-0.14	0.22-0.15	0.14	0.20
Beam loading parameter	[%]	δ	0.0	14.3	16.1	20.6	25.9	9.0	18.2
Peak RF power at section input	[MWatts]	P_s	0.213?	73?	165	130?	150?	120	112.5
RF pulse length	[μsec]	Δ_t	1315?	1.30	0.485	0.250	0.210	0.110	0.065
RF pulse compression ratio	[-]	-	1	?	5	2	3.3	4.55	1
Total number of klystrons or drive	[-]	N_k	1232	4904	5864	8964	9456	2800	2-8
AC to RF efficiency	[%]	η^{Ac}	35	37	30.2	30	37	39	40
RF to beam efficiency	[%]	η^{RF}_{beam}	40	11.1	19.5	20.4	21.3	21.5	29.7
AC to beam efficiency	[%]	η^{AC}	14	4.1	5.9	6.1	7.9	8.4	11.9
AC power for RF generation	[MW]	P_{ac}	140	284	133	234	191	114	143
Figure of Merit	$10^{37}cm^{-2}s^{-1}A^{-1}$	M	26.5	4.4	9.7	11.4	16.3	11.0	13.8

Appendix 1

Definition of parameters

Beam parameters:

L	$\left[m^{-2}s^{-1}\right]$	luminosity
M	$\left[m^{-2}s^{-1}I^{-1}\right]$	normalised luminosity or figure of merit
k_b	$[-]$	number of bunches per linac
N_b	$[-]$	number of particles per bunch
f_{rep}	$[Hz]$	linac repetition frequency
P_b	$[W]$	beam power per linac
W_b	$[J]$	overall beam energy per linac pulse
q_b	$[C]$	charge per bunch
Δ_b	$[s]$	interval between bunches
U_f	[eV]	beam energy at the Interaction Point (I.P.)
U_o	[eV]	beam energy at injection into the main linac
σ_x^*	$[m]$	r.m.s. horizontal beam size at Interaction Point (I.P.)
σ_y^*	$[m]$	r.m.s. vertical beam size at Interaction Point (I.P.)
$\overline{\sigma}_{x,y}^*$	$[m]$	effective r.m.s. transverse beam size with pinch effect during collision
$\varepsilon_{nx,yo}$	$[rad-m]$	r.m.s. transverse normalized beam emittance at injection into linac
$\varepsilon_{nx,y}$	$[rad-m]$	r.m.s. transverse normalized beam emittance at the end of the linac
$\varepsilon_{nx,y}^*$	$[rad-m]$	r.m.s. transverse normalized beam emittance at I.P.
$\beta_{x,y}^*$	$[m]$	r.m.s. transverse Twiss beta function at Interaction Point
$<\beta_o>$	$[m]$	r.m.s. mean Twiss beta function at injection into main linac
α	$[-]$	scaling of beam focusing optics along main linac
σ_z	$[m]$	r.m.s. bunch length
$D_{x,y}$	$[-]$	disruption parameters in transverse planes
D	$[-]$	overall beam disruption parameter
$H_{Dx,y}$	$[-]$	luminosity enhancement parameters in transverse planes
H_D	$[-]$	overall luminosity enhancement parameter
δ_B	[%]	relative beam energy loss induced by beamstrahlung
n_γ	$[-]$	number of photons emitted by beamstrahlung per electron
Y	$[-]$	beamstrahlung parameter

RF parameters:

η_b^{AC}	$[\%]$	wall plug to beam power transfer efficiency
η_{RF}^{AC}	$[\%]$	wall plug to RF transfer efficiency
η_b^{RF}	$[\%]$	RF to beam power transfer efficiency
W_{RF}	$[J]$	RF energy per linac pulse
N_S	$[-]$	number of accelerating structures per linac
W_S	$[J]$	RF energy per accelerating structure and linac pulse
ω	$[Hz]$	RF frequency of accelerating structure
U_S	$[eV]$	beam energy gain per accelerating structure
Δ_f	$[s]$	filling time of accelerating structure
L_S	$[m]$	length of accelerating structure
P_f	$[W]$	RF power during filling of accelerating structures
P_t	$[W]$	RF power during acceleration of train of bunches
G_a	$[V/m]$	loaded mean accelerating field
G_u	$[V/m]$	unloaded mean accelerating field
G_f	$[V/m]$	mean accelerating field respectively during the RF fill
τ	$[-]$	field attenuation constant of accelerating structure
R	$[\Omega]$	shunt impedance of accelerating structure
R'	$[\Omega/m]$	shunt impedance per meter of accelerating structure
$r = R/Q$	$[\Omega]$	normalized shunt impedance of accelerating structure
$r' = R'/Q$	$[\Omega/m]$	normalized shunt impedance per meter of accelerating structure
Q	$[-]$	quality factor of accelerating structure
a/λ	$[-]$	ratio of iris radius of accelerating structure to RF wavelength
v_g/c	$[\%]$	ratio of group velocity in accelerating structure to light velocity
δ	$[\%]$	beam loading parameter in accelerating structure
J, J_u	$[-]$	beam current normalised to the loaded, unloaded gradient.

Constants:

$c = 2.997925$ ms^{-1}	velocity of light
$e = 1.602 \times 10^{23}$ C	charge of electron
$U_e = 511$ keV	rest energy of electron
$\alpha_e = 7.2993 \times 10^{-3}$	fine structure constant (1/137)
$\lambda_e = 3.8616 \times 10^{-13}$	Compton wavelength
$r_e = 2.8179 \times 10^{-15}$ m	classical radius of electron
$\mu_o = 4\pi \times 10^{-7}$ Hm^{-1}	permeability of free space
$\varepsilon_o = \left(\mu_o c^2\right)^{-1}$ Fm^{-1}	permittivity of free space

Appendix 2

The Luminosity and its limitations

The luminosity is given as follows:

$$L = \frac{k_b N_b^2 f_{rep}}{4\pi \bar{\sigma}_x^* \bar{\sigma}_y^*} = \frac{N_b P_b}{4\pi e U_f \bar{\sigma}_x^* \bar{\sigma}_y^*} = \frac{H_D}{4\pi e} \frac{N_b}{U_f} \frac{P_b}{\sigma_x^* \sigma_y^*} \qquad \text{(A2-1)}$$

where P_b is the beam power per linac:

$$P_b = k_b q_b U_f f_{rep} = k_b N_b e U_f f_{rep} \qquad \text{(A2-2)}$$

and following [2,3]:

- σ_x^*, σ_y^*, are the nominal horizontal and vertical r.m.s. beam sizes respectively and are calculated from the normalized beam emittances, ε_{nx}^*, ε_{ny}^*, respectively before collision at the I.P.

$$\varepsilon_{nx}^* = \frac{U_f}{U_e} \frac{\sigma_x^{*2}}{\beta_x^*} \quad \text{and} \quad \varepsilon_{ny}^* = \frac{U_f}{U_e} \frac{\sigma_y^{*2}}{\beta_y^*}$$

- $\bar{\sigma}_x^* = \frac{\sigma_x^*}{\left(H_{Dx}\right)^{1/2}}$ and $\bar{\sigma}_y^* = \frac{\sigma_y^*}{\left(H_{Dy}\right)^{f(\frac{\sigma_x^*}{\sigma_y^*})}}$ are the effective r.m.s. horizontal and vertical beam sizes respectively during collision at the Interaction Point (I.P.)

- $H_D = \left(H_{Dx}\right)^{1/2} \left(H_{Dy}\right)^{f\left(\frac{\sigma_x^*}{\sigma_y^*}\right)}$ is the disruption parameter and $f(u) = \frac{1+2u^3}{6u^3}$

- $H_{Dx,y} = 1 + D_{x,y}^{1/4} \left(\frac{D_{x,y}^3}{1+D_{x,y}^3} \right) \left[\ln\left(\sqrt{D_{x,y}} + 1 \right) + 2\ln\left(\frac{0.8\beta_{x,y}^*}{\sigma_z} \right) \right]$

- $D_{x,y} = \frac{2 r_e N_b \sigma_z}{\gamma \sigma_{x,y}^* \left(\sigma_x^* + \sigma_y^* \right)}$ (A2-3)

Using the above expressions gives:

- $\bar{\sigma}_x^* = \dfrac{\sigma_x^*}{(H_{Dx})^{1/2}} = \dfrac{U_e^{1/2}\varepsilon_{nx}^{*1/2}\beta_x^{*1/2}}{U_f^{1/2}(H_{Dx})^{1/2}}$ (A2-4)

- $\bar{\sigma}_y^* = \dfrac{\sigma_y^*}{(H_{Dy})^{f(\frac{\sigma_x^*}{\sigma_y^*})}} = \dfrac{U_e^{1/2}\varepsilon_{ny}^{*1/2}\beta_y^{*1/2}}{U_f^{1/2}(H_{Dy})^{f(\frac{\sigma_x^*}{\sigma_y^*})}}$ (A2-5)

The intensity of the beam-beam interaction is characterised by the following three parameters [3]:

(i) The beamstrahlung parameter, Υ, which is proportional to the ratio of the critical energy, $\hbar\omega_c$, of the photons emitted in the collision to the energy of the electrons before radiation:

$$\Upsilon = \frac{2}{3}\frac{\hbar\omega_c}{U_f} = \frac{5}{6}\frac{r_e}{\alpha_e U_e}\frac{U_f}{\sigma_z}\frac{N_b}{(\bar{\sigma}_x^* + \bar{\sigma}_y^*)} \qquad \text{(A2-6)}$$

(ii) The relative energy loss, δ_B, induced by beamstrahlung,

$$\delta_{B\cong} \cong \left\langle -\frac{\Delta E}{E} \right\rangle \cong 1.24\frac{\alpha_e\sigma_z U_e}{\lambda_e U_f}\frac{\Upsilon^2}{\left[1+(1{,}5\Upsilon)^{2/3}\right]^2} \qquad \text{(A2-7)}$$

(iii) The number of photons emitted per electron

$$n_\gamma \cong 2.54\frac{\alpha_e\sigma_z U_e}{\lambda_e U_f}\frac{\Upsilon}{\left(1+\Upsilon^{2/3}\right)^{1/2}} \qquad \text{(A2-8)}$$

In a Linear Collider, the luminosity is usually limited by the values of relative energy loss and/or the number of emitted photons per electron that can be tolerated.

A2-1. Low beamstrahlung regime (Y << 1):

In low energy linear colliders where the beamstrahlung energy loss parameter δ_B is usually limited to a few percent to obtain a narrow luminosity spectrum and $\Upsilon << 1$, expressions (A2-7) and (A2-8) become:

$$\delta_B \cong \left\langle -\frac{\Delta E}{E} \right\rangle \cong 1.24\frac{\alpha_e U_e\sigma_z\Upsilon^2}{\lambda_e U_f} \qquad \text{(A2-9)}$$

$$n_\gamma \cong 2.54\frac{\alpha_e U_e\sigma_z\Upsilon}{\lambda_e U_f} \qquad \text{(A2-10)}$$

or substituting for Y from (A2-9)

$$n_\gamma \cong 2.28\left(\frac{\alpha_e U_e \sigma_z \delta_B}{\lambda_e U_f}\right)^{1/2} \qquad \text{(A2-11)}$$

Replacing the beamstrahlung parameter, Y , in (A2-9) and (A2-10) by its expression in (A2-6) :

$$\delta_B \cong 0.86 \frac{r_e^2}{\lambda_e \alpha_e U_e} \frac{U_f}{\sigma_z} \frac{N_b^2}{\left(\bar{\sigma}_x^* + \bar{\sigma}_y^*\right)^2} \qquad \text{(A2-12)}$$

$$n_\gamma \cong 2.12 \frac{r_e}{\lambda_e} \frac{N_b}{\left(\bar{\sigma}_x^* + \bar{\sigma}_y^*\right)} \qquad \text{(A2-13)}$$

Rewriting (A2-12) in terms of the charge per bunch :

$$N_b \propto \frac{\sigma_z^{1/2}\left(\bar{\sigma}_x^* + \bar{\sigma}_y^*\right)}{U_f^{1/2}} \delta_B^{1/2} \qquad \text{(A2-14)}$$

Alternatively substituting in (A2-14) for δ_B using (A2-11) gives:

$$N_b \propto n_\gamma \left(\bar{\sigma}_x^* + \bar{\sigma}_y^*\right) \qquad \text{(A2-15)}$$

Substituting for N_b in (A2-1) using either (A2-14) or (A2-15), the luminosity becomes:

$$L \propto \frac{\delta_B^{1/2} \sigma_z^{1/2}}{U_f^{3/2}} \left(\frac{1}{\bar{\sigma}_x^*} + \frac{1}{\bar{\sigma}_y^*}\right) P_b \propto \frac{n_\gamma}{U_f} \left(\frac{1}{\bar{\sigma}_x^*} + \frac{1}{\bar{\sigma}_y^*}\right) P_b \qquad \text{(A2-16)}$$

This general expression for luminosity (A2-16) is greatly simplified when the following two approximations are made, which are valid in all practical linear collider designs:

First approximation: $\bar{\sigma}_y^* << \bar{\sigma}_x^*$

In order to limit the beam energy spread induced by beamstrahlung whilst at the same time maximising the luminosity, the vertical size of the beam at the interaction point is made much smaller than the horizontal one. In this case with $\bar{\sigma}_y^* << \bar{\sigma}_x^*$ in (A2-16):

$$L \propto \frac{\delta_B^{1/2}}{U_f^{3/2}} \frac{\sigma_z^{1/2}}{\bar{\sigma}_y^*} P_b \propto \frac{n_\gamma}{U_f} \frac{P_b}{\bar{\sigma}_y^*} \qquad \text{(A2-17)}$$

with $\delta_B \cong 0.86 \frac{r_e^2}{\lambda_e \alpha_e U_e} \frac{U_f}{\sigma_z} \frac{N_b^2}{\overline{\sigma}_x^{*2}}$ and $n_\gamma \cong 2.12 \frac{r_e}{\lambda_e} \frac{N_b}{\overline{\sigma}_x^*}$ (A2-18)

Second approximation: $\beta_y^* = \sigma_z$

In order to limit the reduction in luminosity by the "hourglass" effect at the interaction point, the Beta function in the vertical plane is chosen to be equal to the bunch length. In this case, with $\beta_y^* = \sigma_z$, and using (A2-5) in (A2-17) :

$$L \propto \left(H_{Dy}\right)^{f\left(\frac{\sigma_x^*}{\sigma_y^*}\right)} \frac{\delta_B^{1/2}}{U_f} \frac{P_b}{\varepsilon_{ny}^{*1/2}} \propto \left(H_{Dy}\right)^{f\left(\frac{\sigma_x^*}{\sigma_y^*}\right)} \frac{n_\gamma}{U_f^{1/2}} \frac{P_b}{\beta_y^{*1/2} \varepsilon_{ny}^{*1/2}} \qquad \text{(A2-19)}$$

Conclusion of the low beamstrahlung regime:

In the case of the low beamstrahlung regime, for a fixed beam power, the normalized vertical beam emittance is the only beam parameter which can be optimized to improve the luminosity without deterioration by beamstrahlung of the relative energy loss, δ_B, and the number of emitted photons per electron, n_γ.

A2-2. High beamstrahlung regime (Y >> 1):

In high energy linear colliders ($U_{cm} = 2U_b > 3$ TeV) where the beamstrahlung parameter Y >> 1, (A2-7) and (A2-8) become:

$$\delta_{B\cong} \cong \left\langle -\frac{\Delta E}{E} \right\rangle \cong 0.72 \frac{\alpha_e U_e \sigma_z \mathrm{Y}^{2/3}}{\lambda_e U_f} \text{ and } n_\gamma \cong 2.54 \frac{\alpha_e U_e \sigma_z \mathrm{Y}^{2/3}}{\lambda_e U_f} \Rightarrow n_\gamma \cong 3.5 \delta_B \text{ (A2-20)}$$

Replacing in (A2-20), the beamstrahlung parameter from its expression in (A2-6) :

$$\delta_B \cong \frac{n_\gamma}{3.5} \cong 0.64 \frac{r_e^{2/3} \alpha_e^{1/3} U_e^{1/3}}{\lambda_e} \frac{\sigma_z^{1/3}}{U_f^{1/3}} \frac{N_b^{2/3}}{\left(\overline{\sigma}_x^* + \overline{\sigma}_y^*\right)^{2/3}} \qquad \text{(A2-21)}$$

Rewriting (A2-21) in terms of the charge per bunch :

$$N_b \propto \frac{U_f^{1/2} \left(\overline{\sigma}_x^* + \overline{\sigma}_y^*\right)}{\sigma_z^{1/2}} \delta_B^{3/2} \propto \frac{U_f^{1/2} \left(\overline{\sigma}_x^* + \overline{\sigma}_y^*\right)}{\sigma_z^{1/2}} n_\gamma^{3/2} \qquad \text{(A2-22)}$$

Using (A2-22) in (A2-1), the luminosity becomes:

$$L \propto \frac{\delta_B^{3/2}}{U_f^{1/2}} \left(\frac{1}{\overline{\sigma}_x^*} + \frac{1}{\overline{\sigma}_y^*} \right) \frac{P_b}{\sigma_z^{1/2}} \propto \frac{n_\gamma^{3/2}}{U_f^{1/2}} \left(\frac{1}{\overline{\sigma}_x^*} + \frac{1}{\overline{\sigma}_y^*} \right) \frac{P_b}{\sigma_z^{1/2}} \qquad \text{(A2-23)}$$

This general expression for luminosity (A2-23) is again greatly simplified when the two approximations, $\overline{\sigma}_y^* << \overline{\sigma}_x^*$ and $\beta_y = \sigma_z$, are made.

First approximation: $\overline{\sigma}_y^* << \overline{\sigma}_x^*$

With $\overline{\sigma}_y^* << \overline{\sigma}_x^*$, in (A2-23):

$$L \propto \frac{\delta_B^{3/2}}{U_f^{1/2}} \frac{P_b}{\overline{\sigma}_y^* \sigma_z^{1/2}} \propto \frac{n_\gamma^{3/2}}{U_f^{1/2}} \frac{P_b}{\overline{\sigma}_y^* \sigma_z^{1/2}} \qquad \text{(A2-24)}$$

$$\text{with} \quad \delta_B \cong \frac{n_\gamma}{3.5} \cong 0.64 \frac{r_e^{2/3} \alpha_e^{1/3} U_e^{1/3}}{\lambda_e} \frac{\sigma_z^{1/3}}{U_f^{1/3}} \frac{N_b^{2/3}}{\overline{\sigma}_y^{*2/3}} \qquad \text{(A2-25)}$$

Second approximation: $\beta_y^* = \sigma_z$

With $\beta_y^* = \sigma_z$, and introducing (A2-5) in (A2-24):

$$L \propto \left(H_{Dy}\right)^f \left(\frac{\sigma_x^*}{\sigma_y^*}\right) \delta_B^{3/2} \frac{P_b}{\sigma_z \varepsilon_{ny}^{*1/2}} \propto \left(H_{Dy}\right)^f \left(\frac{\sigma_x^*}{\sigma_y^*}\right) n_\gamma^{3/2} \frac{P_b}{\sigma_z \varepsilon_{ny}^{*1/2}} \qquad \text{(A2-26)}$$

However, it should be noted that attaining the very small beta functions suggested in these scaling laws may be impossible for the final focus system. Thus, in the body of this report and in the case of high beamstrahlung regime, we will assume that β_y^* is determined by the performance of the final focus with:

$$\beta_y^* = Const. \geq \sigma_z$$

Conclusion of the high beamstrahlung regime:

In the special case of the high beamstrahlung regime inherent in very high energy linear colliders, short bunches are particularly favorable as they improve the luminosity while minimizing at the same time both the relative energy loss, δ_B , and the number of emitted photons per electron, n_γ , induced by beamstrahlung.

Appendix 3

RF to beam transfer efficiency

The RF to beam transfer efficiency in a linac of N_S constant gradient travelling wave accelerating structures of length, L_s, accelerating a beam of k_b bunches each of charge, q_b ,is given by:

$$\eta_b^{RF} = \frac{W_b}{W_{RF}} \qquad \text{(A3-1)}$$

where W_b is the total energy taken out by the beam, and W_{RF} is the total RF input energy to the linac.
Each accelerating structure is fed by an RF energy, W_S, to provide a beam acceleration per structure, U_S ,

$$W_b = N_S k_b q_b U_S \qquad \text{(A3-2)}$$

$$W_{RF} = N_S W_S \qquad \text{(A3-3)}$$

The RF to beam transfer efficiency for the whole linac is the same as that for each accelerating structure:

$$\eta_b^{RF} = \frac{W_b}{W_{RF}} = \frac{k_b q_b U_S}{W_S} \qquad \text{(A3-4)}$$

Assuming a linear ramp of the RF before injection of the beam to compensate beam loading along the train of bunches [14], the RF energy to be provided to each accelerating structure is given by:

$$W_S = P_f \Delta_f + P_t \left(N_b - 1\right)\Delta_b \qquad \text{(A3-5)}$$

where the first term is the necessary RF energy to fill the structure and the second term is the RF energy to maintain the accelerating field during acceleration of the train of bunches.
From [4,15]:

$$P_{f,t} = \frac{G_{f,u}^2 l_s^2}{\left(1 - e^{-2\tau}\right)R} \quad \text{and} \quad \Delta_f = \frac{2Q\tau}{\omega} \qquad \text{(A3-6)}$$

where G_f is the mean field during the filling time of the structure and is equal to the loaded accelerating field, G_a. G_u is the unloaded accelerating field during acceleration. G_d is the decelerating field induced by the passage of the bunches:

$$G_f \cong G_a \quad \text{and} \quad G_u = \left(G_a + G_d\right) \tag{A3-7}$$

where, following [15]:

$$G_d = \frac{R' q_b}{2\Delta_b}\left(1 - \frac{e^{-2\tau}}{g(\tau)}\right) \quad \text{and} \quad g(\tau) = \frac{1 - e^{-2\tau}}{2\tau} \tag{A3-8}$$

Putting (A3-6), (A3-7) and (A3-8) in (A3-5) and introducing the beam energy increase by each accelerating structure, $U_s = G_a L_s$:

$$W_s = \frac{G_a U_s Q}{\omega g(\tau) R'}\left[1 + \frac{(k_b - 1)\Delta_b \omega}{2\tau Q}\left(1 + \frac{G_d}{G_a}\right)^2\right] \tag{A3-9}$$

The first term in the bracket of expression (A3-9) corresponds to the RF energy required to fill the structure, the second term corresponds to the RF energy needed to keep the structure filled during the passage of the train of bunches and the third term is the compensation for beam loading.

Introducing (A3-9) in (A3-4), the RF to beam efficiency becomes:

$$\eta_b^{RF} = \frac{W_b}{W_{RF}} = \frac{k_b q_b g(\tau) R' \omega}{G_a Q\left\{1 + \frac{(k_b - 1)\Delta_b \omega}{2Q\tau}\left[1 + \frac{G_d}{G_a}\right]^2\right\}} \tag{A3-10}$$

The RF to beam efficiency can also be expressed as a function of the beam loading parameter, δ, which is the ratio of the field reduction by beam loading to the unloaded accelerating field:

$$\delta = \frac{G_u - G_a}{G_u} = 1 - \frac{G_a}{G_u} = \frac{G_d}{G_u} = \frac{1}{1 + \frac{G_a}{G_d}} \tag{A3-11}$$

Replacing in the equation (A3-11) the expression for G_d from equation (A3-8), the beam loading parameter becomes:

$$\delta = \frac{R' q_b}{2 G_u \Delta_b}\left[1 - \frac{e^{-2\tau}}{g(\tau)}\right] = \frac{J_u}{2}\left[1 - \frac{e^{-2\tau}}{g(\tau)}\right] \tag{A3-12}$$

or alternatively:

$$\delta = \frac{\frac{J}{2}\left[1 - \frac{e^{-2\tau}}{g(\tau)}\right]}{1 + \frac{J}{2}\left[1 - \frac{e^{-2\tau}}{g(\tau)}\right]} \qquad \text{(A3-13)}$$

where, J and J_u, are defined as the normalised beam currents:

$$J = \frac{R'q_b}{G_a\Delta_b} \quad \text{and} \quad J_u = J(1-\delta) = \frac{R'q_b}{G_u\Delta_b} \qquad \text{(A3-14)}$$

Expressing the charge per bunch, q_b, as a function of the beam loading parameter by replacing (A3-8) in (A3-11):

$$q_b = \frac{2\Delta_b G_a}{R'\left[1 - \frac{e^{-2\tau}}{g(\tau)}\right]} \times \frac{\delta}{1-\delta} \qquad \text{(A3-15)}$$

Introducing (A3-11) and (A3-12) in (A3-10), the RF to beam efficiency is given by:

$$\eta_b^{RF} = \frac{2g(\tau)}{\left[1 - \frac{e^{-2\tau}}{g(\tau)}\right]} \times \frac{k_b\Delta_b\omega}{Q\left[1 + \frac{(k_b-1)\Delta_b\omega}{2Q\tau(1-\delta)^2}\right]} \times \frac{\delta}{(1-\delta)} \qquad \text{(A3-16)}$$

The expression for the RF to beam efficiency is greatly simplified for the two extreme cases of a single bunch, and for an infinite number of bunches:

The case of a single bunch:

Replacing, $k_b = 1$, in (A3-10):

$$\eta_b^{RF} = \frac{W_b}{W_{RF}} = \frac{g(\tau)R'q_b\omega}{G_aQ} \qquad \text{(A3-17)}$$

Assuming the following well known dependence of the accelerating structure parameters with the RF frequency [4]:

$$R' \propto \omega^{1/2}(a/\lambda)^{-1} \quad \text{and} \quad Q \propto \omega^{-1/2} \qquad \text{(A3-18)}$$

the RF to beam efficiency for the case of a single bunch increases with the square of the RF frequency for a given charge and is inversely proportional to the accelerating gradient :

$$\eta_b^{RF} = \frac{W_b}{W_{RF}} = \frac{g(\tau) q_b \omega^2}{G_a(a/\lambda)} \qquad \text{(A3-19)}$$

The variation of the function g(τ) with the accelerating structure field attenuation constant, τ, as displayed in Fig.A1 shows that short structures give the highest RF to beam efficiency for single bunch operation.

The case of an infinite number of bunches:

Replacing, $k_b = \infty$, in (A3-16) and using expression (A3-12):

$$\eta_b^{RF} = \frac{4\tau g(\tau)}{\left[1 - \frac{e^{-2\tau}}{g(\tau)}\right]} \delta(1-\delta) = 2\tau g(\tau) J_u \left[1 - \frac{J_u}{2}\left(1 - \frac{e^{-2\tau}}{g(\tau)}\right)\right] \qquad \text{(A3-20)}$$

or using expression (A3-13):

$$\eta_b^{RF} = \frac{2\tau g(\tau) J}{\left[1 + \frac{J}{2}\left(1 - \frac{e^{-2\tau}}{g(\tau)}\right)\right]^2} \qquad \text{(A3-21)}$$

It is remarkable that for an infinite number of bunches, the RF to beam efficiency becomes independent of the RF frequency, of the charge per bunch and of the accelerating gradient, and that it only depends on two parameters, the field attenuation per accelerating structure and either the beam loading parameter or the dimensionless beam current.

The variation of the RF to beam efficiency with τ for a fixed beam loading is shown in Fig. A1, and the variation with δ for different values of τ in Fig. A2. It can be seen from Fig. A2 that the maximum RF to beam efficiency always occurs at δ = 0.5 that is to say when the average loaded accelerating field is half the average unloaded field. Very high efficiencies close to 100% can be obtained with very short structures but require strong beam currents as shown in Fig. A3 which displays the variation of the RF to beam efficiency as a function of the normalised beam current, J_u, for various values of the structure field attenuation parameter. It is seen on Fig. A4 that for increasing beam currents, the RF to beam efficiency goes through a maximum for an optimum value, τ_{opt}, of the field attenuation parameter, or length of the structure. τ_{opt} is obtained by derivation of equation (A3-20):

$$\frac{d\eta_b^{RF}}{d\tau} = 2J_u e^{-2\tau_{opt}}\left(1 - J_u \tau_{opt}\right) = 0 \quad \Rightarrow \quad \tau_{opt} = \frac{1}{J_u} = \frac{1}{J(1-\delta)} \qquad \text{(A3-22)}$$

The corresponding optimum efficiency is shown in Fig. A5 together with the associated optimum field attenuation parameter, and the corresponding beam loading as a function of the parameter, J_u.

Fig. A1: Variation of the main RF efficiency functions with the field attenuation per accelerating structure

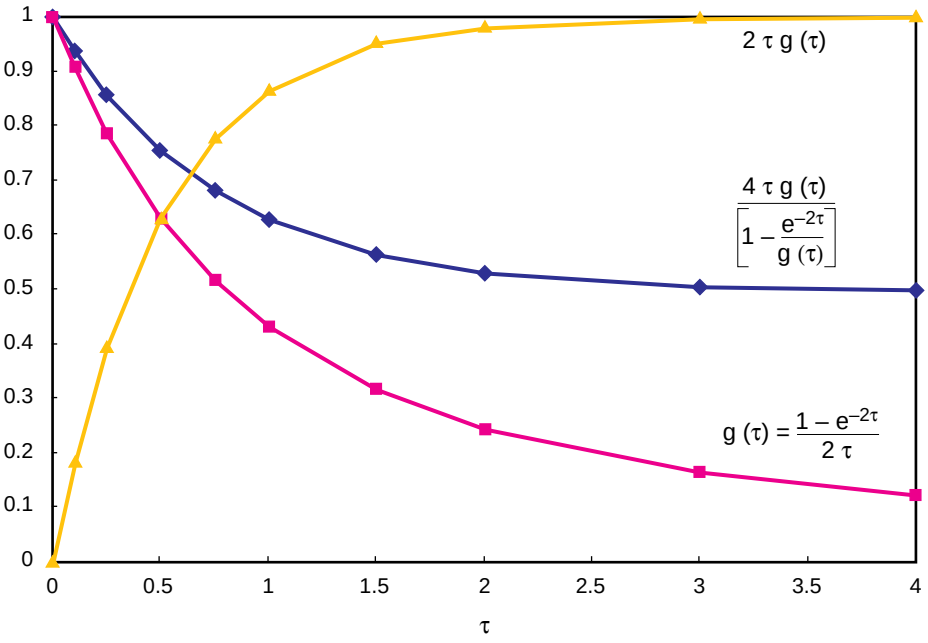

Fig. A2: RF to beam efficiency as a function of the beam loading parameter

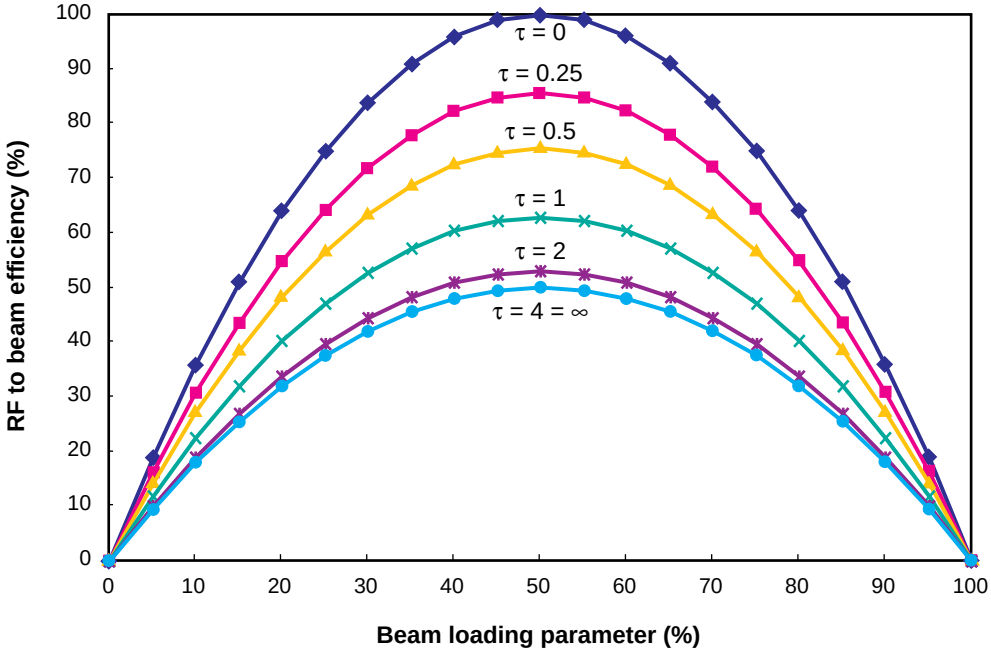

These curves are of a very general interest as they are fully independent of beam and linac parameters with thee only assumption of the extreme case of an infinite number of bunches:

Fig. A3: RF to beam efficiency as a function of the normalized beam current

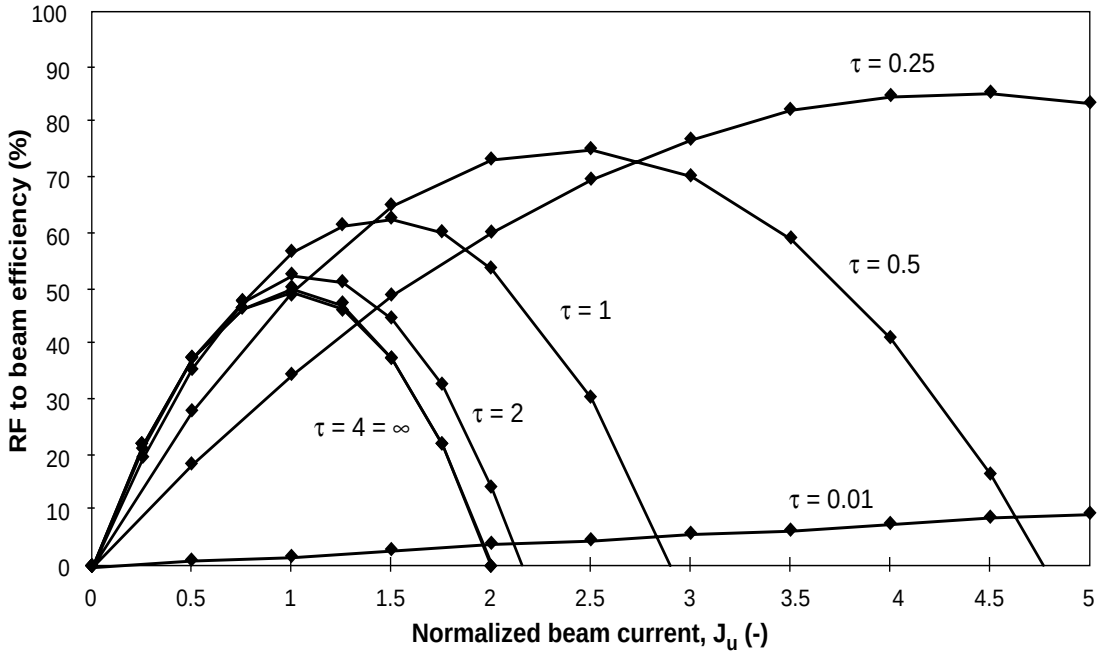

Fig. A4: RF to beam efficiency as a function of the field attenuation of the structures

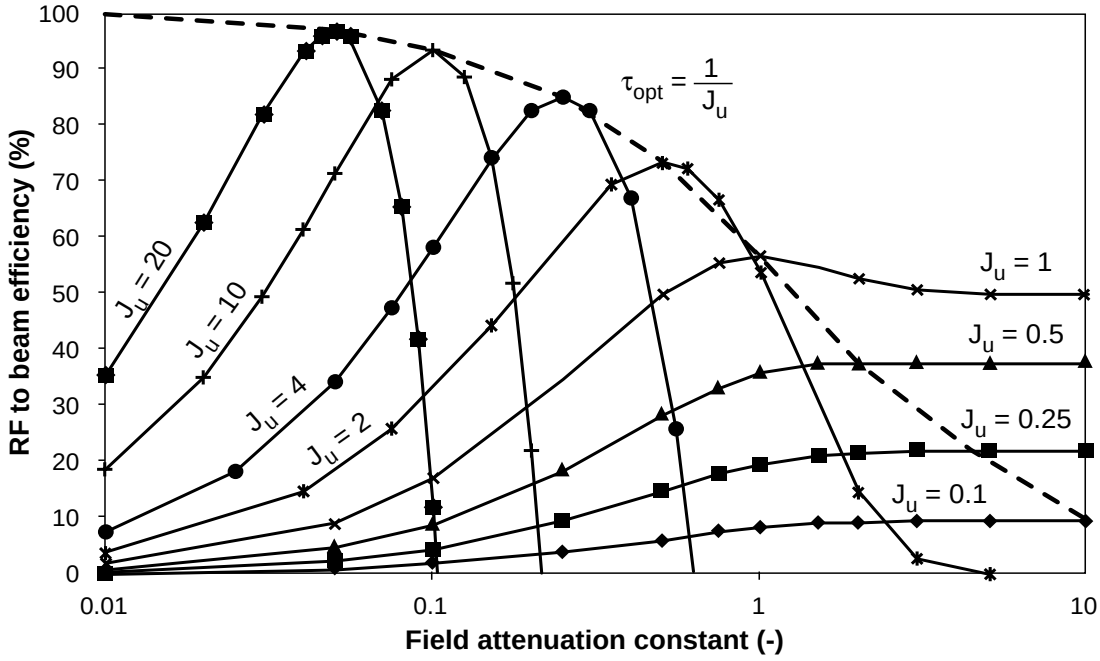

Fig. A5: Optimum RF to beam efficiency and beam loading parameters versus the normalized beam current